NUMERICAL ANALYSIS OF THERMAL SPRAY COATING PROCESS

Raja jayasingh.T

A Dissertation Submitted to
Indian Institute of Technology Hyderabad
In Partial Fulfillment of the Requirements for
The Degree of Master of Technology

भारतीय प्रौद्योगिकी संस्थान हैदराबाद
Indian Institute of Technology Hyderabad

Department of Mechanical Engineering

June, 2012

Declaration

I declare that this written submission represents my ideas in my own words, and where others' ideas or words have been included, I have adequately cited and referenced the original sources. I also declare that I have adhered to all principles of academic honesty and integrity and have not misrepresented or fabricated or falsified any idea/data/fact/source in my submission. I understand that any violation of the above will be a cause for disciplinary action by the Institute and can also evoke penal action from the sources that have thus not been properly cited, or from whom proper permission has not been taken when needed.
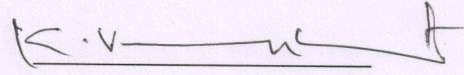
Rajajayasingh.

(Signature)
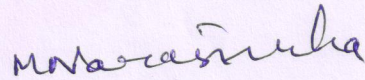
(T.Raja jaya singh)

(me10m09)

1

Approval Sheet

This thesis entitled "Numerical Analysis of Thermal Spray Coating Process" by Raja jaya singh.T is approved for the degree of Master of Technology from IIT Hyderabad.

Dr.K.Venkatasubbaiah

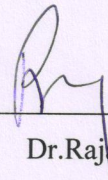Assistant Professor

Examiner
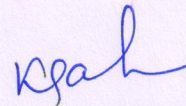
Dr.Narasimha Mangadoddy

Assistant Professor

Examiner

Dr.Raja Banerjee

Assistant Professor

Adviser

Dr.Kirti Chandra Sahu

Assistant Professor

Chairman

Acknowledgement

First, I would like to express my sincere gratitude and appreciation to my supervisor **Dr. Raja Banerjee** for his guidance and constant support throughout the work. Also, for making sure that necessary resources were available. His belief in me and friendly nature helped me to complete this thesis.

I would like to thank Mr.Madhu (Joshua) who helped me in the CAE lab for installing the softwares.

I would also like to thank my parents and family members for their constant support and belief in me. Thanks to all my colleagues, close friends for all the good time that enhanced my studies.

Last but not the least, thanks to God's grace.

Dedicated

to

My Family Members.

Abstract

A numerical study of Thermal spraying process is required for optimizing performance and gun design for spraying various materials. Cold spray process is a new technique of thermal spray process which is used in industries and very limited data is available. This thesis presents an investigation on the powder stream characteristics in cold spray supersonic nozzles. This work describes a detailed study of the various parameters, namely applied gas pressure, gas temperature, size of particles, outlet gas velocity, dimensions of the nozzle on the outlet velocity of the particles. A model of a two-dimensional axisymmetric nozzle was used to generate the flow field of particles (copper or tin) with the help of a carrier gas (compressed) stream like nitrogen or helium flowing at supersonic speed. Particles are dragged by the carrier gas up to high velocity magnitudes, resulting in severe plastic deformation processes upon impact with a solid substrate positioned at the distance SoD (Standoff Distance).

ANSYS FLUENT software was used for the simulation of a cold spray nozzle. A standard k-€ model has been used to account for the turbulence produced due to the very high velocity of flow. The Lagrangian approach (one way coupling) was used for calculating the motion of the particles in DPM modeling. In DPM "high-mach-number" drag law was applied in the simulations. In order to take into account for particle dispersion due to turbulence effects, the Stochastic-Tracking type model implemented in Fluent was used. In this approach, the Discrete Random Walk (DRW) model is used to predict the fluctuating components of the total particle velocity and effects on its trajectory. When the path is computed for a sufficient number of times, a realistic prediction of the random effects by turbulence on particle dynamics can be achieved. Differences in velocity of particles were modeled over the range of applied gas pressure, gas temperature and size of particles. From the CFD simulation results optimum values of gas pressure and temperature were found for making a successful coating of particles. The simulation results show good agreement with previous cold spry work using different spraying materials.

Validation of CFD model was done by compare with the experimental results for the similar flow conditions. The grid quality of the model was investigated to get the results to converge and be independent of the grid size to give good agreement between the accuracy of the results and the computational time. The model was analyzed for different coating thickness of copper and tin ranging from 1mm to 8mm in width on metal and polymer substrates.

Nomenclature

ρ	Fluid Density
ϵ	Dissipation
k	Kinetic Energy
G_k	Generation of Turbulent kinetic Energy
σ_k	Turbulent Prandtl Number For k
σ_ϵ	Turbulent Prandtl number for €
F_X	Force due to Pressure Gradient in the Flow
u	Fluid Phase Velocity
u_p	Particle Velocity
μ	Molecular Viscosity of Fluid
ρ_p	Density of Particle
d_p	Diameter of Particle
R_e	Relative Reynolds Number
u	Mean Fluid Phase Velocity
u'	Fluctuating Velocity
T_{ref}	Reference Temperature
n	Size Distribution Parameter
d	Mean Diameter of Particle
Y_d	Mass fraction of Particle
S	Sutherland Temperature
P	Local Gauge Pressure
P_{OP}	Operating Pressure

Contents

Chapter 1

Introduction

1.1 Background

Over the past few years new spraying techniques for coating purposes have been experimentally and computationally analyzed for better understanding of the thermo-mechanical processes involved. Cold spray technology is attracting the researchers and industries worldwide because of its advantages over the other spraying methods [1]. The cold spray dynamic technology is a new technique for coating metals with very small metal powder particles using compressed gas stream propulsion. This technology was developed with the aim of producing pore free and non oxidized coatings which were not possible with other conventional coating techniques like HVOF, Plasma spraying and arc spraying. Due to the high velocity of particles, this process gives a highly bonded coating with good adhesion between particles and substrate, low friction coefficient, high thermal and electrical conductivity, and excellent corrosion and oxidation resistance [2].

Many companies and researchers worldwide are working on cold spray. In USA, research on cold spray technology was first undertaken by a consortium formed under the auspices of the National Centre for Manufacturing Sciences (NCMS). After that many research centers became interested in this technology e.g. the Institute of Theoretical and Applied Mechanics of the Russian Academy of Science, Sandia National Laboratories and Pennsylvania State University [3]. Sandia National Lab had funded companies like ASB Industries, Ford, K-Tech, Pratt & Whitney to a value of 0.5 million U.S. dollars a year for 3 years to do R&D and develop this technology. Pennsylvania State University have received grants from the U.S. Navy to do R&D on the cold spray process and develop an anti skid coating [4].

1.2 Thermal spraying

Thermal spray is the process in which a metal or alloy in molten or semi molten state is used to make a layer on a substrate. The thermal spray technique was first used in the early 1900s when Dr Schoop (refer to the Master patent of Schoop technology) [5] used a flame as a heat source. Initially it was practiced on metals with low melting point and after that it was progressively extended to metals with high melting point [5]. For making the deposit in thermal spraying a stream of molten metal particles strike a substrate, become flattened and then undergo rapid solidification and quenching. Every droplet spreads to make its own layer and these layers join to make a deposit of thermally sprayed material. In this process voids are formed in the deposit mainly because of incomplete filling or incomplete wetting of the molten metal and during the quenching of brittle materials micro cracks are formed after the solidification of molten material. These affect the mechanical properties like elastic modulus and stress at failure and physical properties like thermal conductivity [6].

1.3 Different Methods of Thermal Spraying

There are different types of thermal spray methods available to make coatings on a substrate, either to improve surface properties for protection against corrosion, wear or as a thermal barrier. The different types of thermal spraying techniques are:-

- HVOF (High Velocity Oxy-fuel Spraying

- Electric Arc Wire Spraying

- Plasma Spraying

- Flame Spraying

- Cold Spraying

1.3.1 HVOF

The Fig.1.1 shows the schematic diagram of High velocity oxy-fuel spraying. In this method in which oxygen and fuel are burnt and then passed through a nozzle with free expansion which results in a supersonic flame gas velocity. By introducing feedstock powder in the hot stream, the powder particles become extremely hot and reach supersonic velocity. The particles flatten after striking the substrate to form a well bonded and dense coating [7]. As, the temperature of the particles impacting on the substrate ranges from 1500 to 2500 K there is thermal degradation of the coating material. It is difficult to control the temperature of the hot jet and its velocity independently and also difficult to optimize the spray parameters because the spraying parameters, such as fuel flow rate, take time to set up [8].
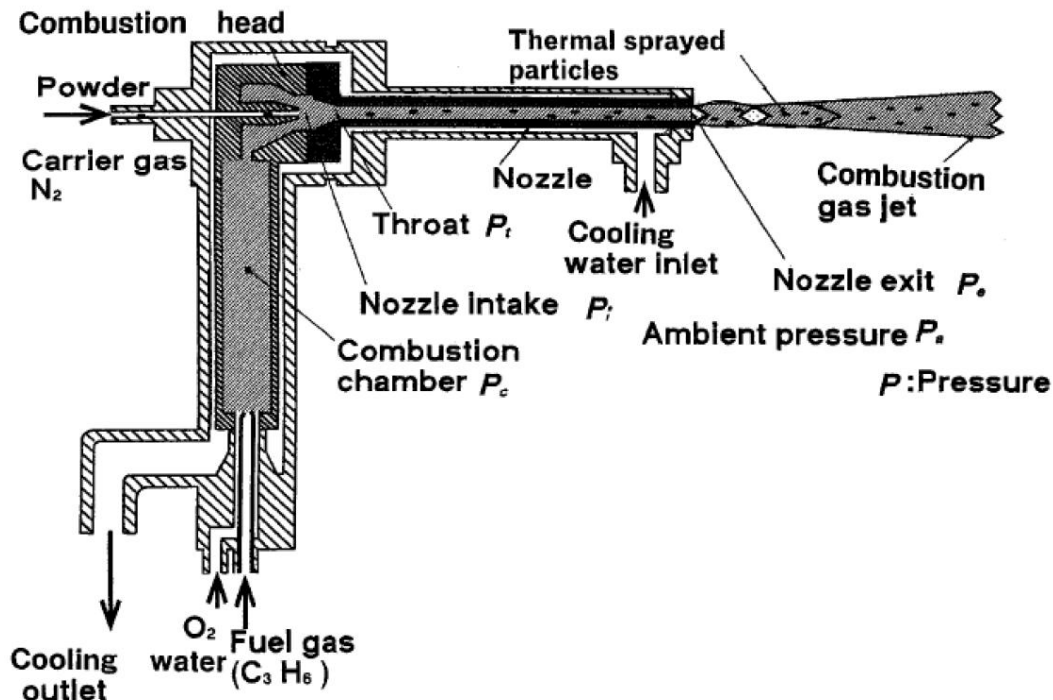
Figure 1.1: Schematic diagram of HVOF apparatus

1.3.2 Electric Arc Wire Spraying

Electric arc wire spraying is a very useful process for making metal coatings because it is a low cost process. The wire used for welding can be electric arc sprayed at high throughput (from 30 to 50kg/hr) [7].
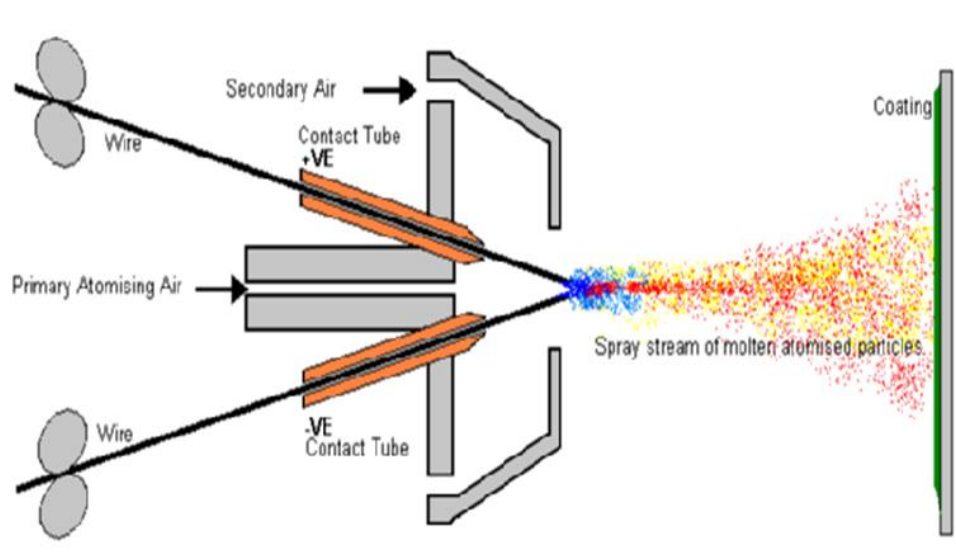
Figure 1.2: Schematic diagram of electric arc wire spraying system

The Fig.1.2 shows the electric arc wire spraying system. Two wires are used in these processes, which are electrically charged, one positively and the other negatively by passing a current through them. The wires are joined to make an arc which melts the wires. Compressed air coming from the nozzle reduces the molten metal to tiny particles and sprays them on the substrate. A higher spray rate can be achieved by using a high current rating system like 350A or 700A [9]. The coating formed by this method has relatively high density and adheres well to the work piece. Greater density and more bond strength can be achieved by carrying out the process in a reduced-pressure chamber [7]. The disadvantage of this process is that only wires

that are electrically conductive can be used and if preheating of the work piece is required then a separate source is necessary in this task [10].

1.3.3 Plasma Spraying

As we can see in the Fig.1.3 the nozzle comprises a tungsten cathode placed axially at the outer part of the anode which is a copper cylinder. A direct current arc is maintained between the axially placed tungsten cathode and the copper anode. An ionized gas is generated by heating it up to a temperature of 50,000°F (30,000°C). The powder is then introduced into the plasma jet where it is heated above its melting temperature and achieves a velocity ranging from 120 to 610 m/sec [10].
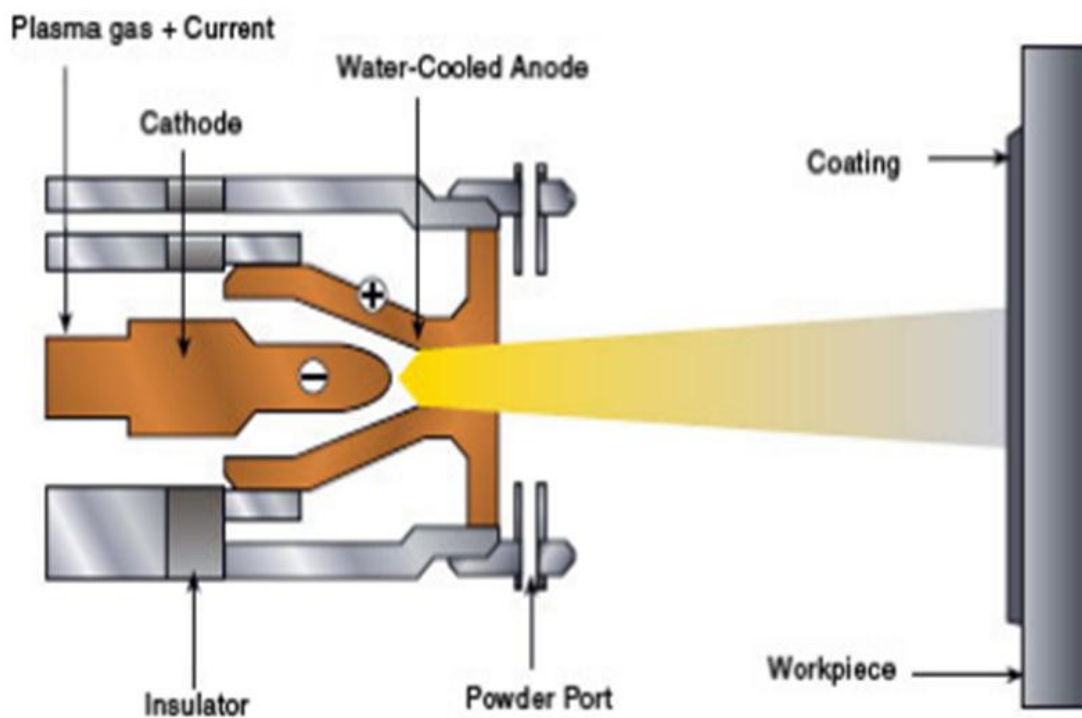
Figure 1.3: Schematic diagram of plasma spraying system

The behaviour of the plasma spraying process is non-deterministic in which molten, semi-molten or sometimes solid particles strike the substrate, flatten followed by solidification and formation of disc-like splats. The size, velocity and thermo physical properties of the particles striking the surface totally influences the splat shape and hence the quality of the coating [11].

1.3.4 Flame Spraying

Standard spraying techniques have certain limitations. It is difficult to make a thin coating on a substrate as in some techniques only certain sizes of powder particles can be used and cannot be reduced from that size, so it is not easy to achieve a homogenous and dense coating. A very good powder feeding technique is needed when using powder particle sizes below 5 μm and these powder qualities are very expensive. Not every combination of material is available in the market [12].
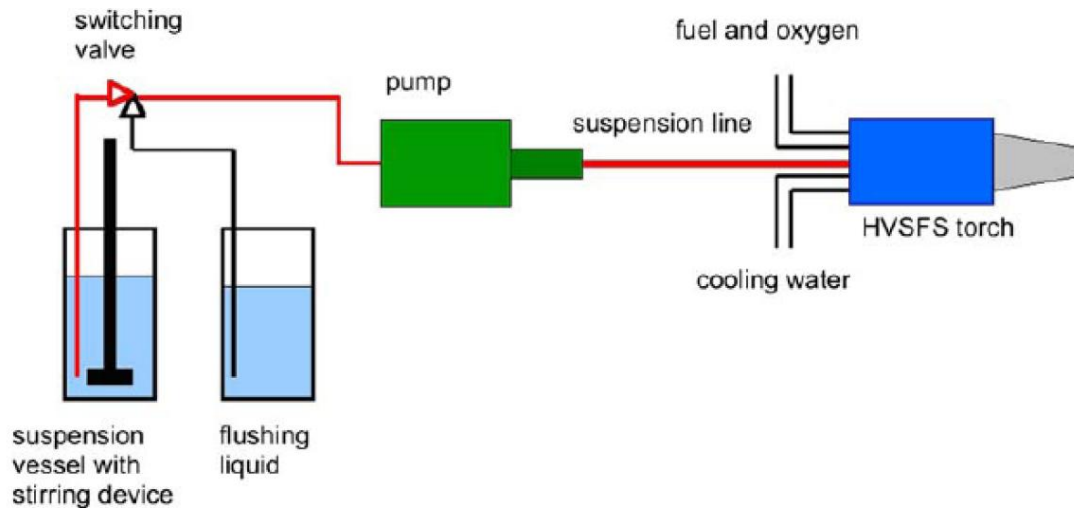
Figure 1.4: Schematic diagram of flame spraying system

High velocity suspension flame spraying is a technique used to spray submicron or nano particles at hypersonic speed to get a dense and thin coating on a work piece. In this process, the powder is mixed with an organic solvent and fed axially into the

combustion chamber or the torch which resembles the High Velocity Oxy-Fuel (HVOF) spray torch [13]. The disadvantage of the HVSFS technique is that for spraying sub-micron sized particles the stand-off distance of the spraying torch has to be very small, which results in heat transfer from the gas jet to the work piece. This heat changes the properties of the piece, so a proper and effective cooling system is required in this process when coating heat sensitive materials [14].

1.4 Cold Spray Process

The phenomenon of cold spray was discovered during an aeronautical investigation in the 1980's. When dusty gases were used in shock tube experiments, the particles were observed to stick on the substrate. This process was undesirable but was recognized to be useful because particles of ductile metals or alloys could be bonded onto metal surfaces, glass or ceramics at impact velocities ranging from 400 to 1200 m/s. This is how coatings are made on work pieces [15].
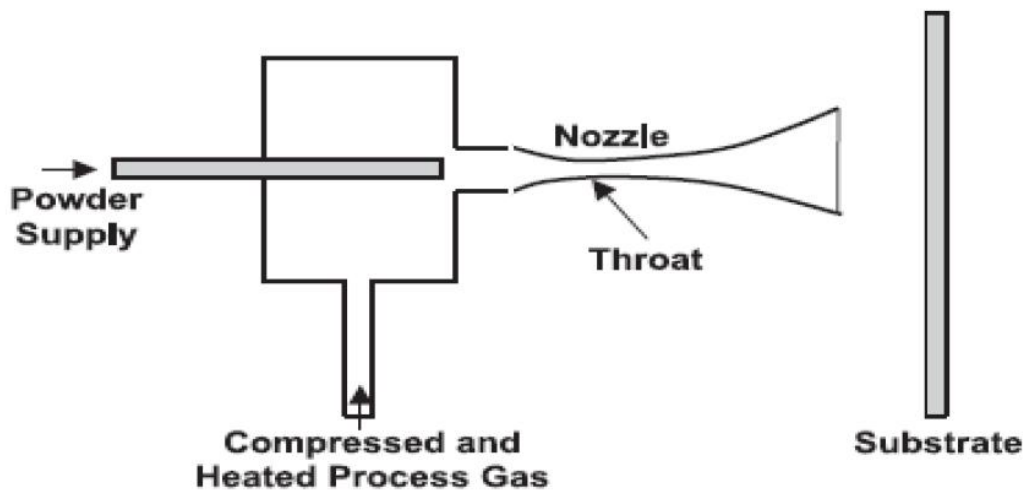
Figure 1.5: Schematic diagram of cold spraying system

The cold spray process or cold gas-dynamic process is a coating process utilizing high speed metal or alloy particles ranging from 1 to 50 μm in size, with a supersonic jet of compressed gas with a velocity ranging from 300 to 1200 m/s on the surface of the work piece is shown in Fig.1.5. The coating formed by this process depends upon a combination of factors like particle velocity, temperature and size. The powder particles in this process are accelerated by a supersonic gas jet at a temperature lower than its melting point, thus reducing many effects which occur in high temperature spraying like oxidation at high temperature, melting of the substrate or spray particles, crystallization, evaporation, stress generation, gas release and other related problems [16].

Studies on cold spraying shows that the most important parameter is the velocity of the particles before they strike the substrate. For making a successful coating the particles should strike the substrate at a higher velocity than a critical velocity [17].
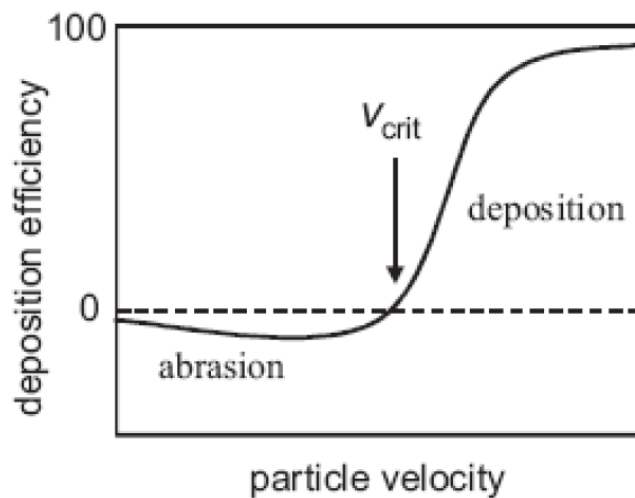
Figure 1.6: Correlation between the particle velocity and deposition efficiency

If the particles strike the substrate at a velocity lower than the critical velocity then the particles will just scratch the surface of the substrate as they do in grit blasting. By increasing the particle velocity the deposition efficiency reaches saturation point

which is nearer to 100%. Most of the research related to cold spray is focused on achieving high particle velocity by making new designs of the nozzle used for spraying [17].

1.4.1 Reason for Doing Cold Spraying

In the cold spray process, particles ranging in size from 5 to 50μm are used to make a coating by number of layers. The cold spray process is relatively better for making thicker coatings than thermal spraying because there are no thermal stresses involved in it [18].

A most important consideration in introducing new process to industry is a reduction in the manufacturing cost of components. Most components in industry are fabricated by casting which is the initial step in the production line. The Pratt & Whitney Company as a part of the US Air Force forging supplier has developed a model called value stream analysis which shows that reduction in cost cannot be achieved by reducing the cost of one area in a production line. Pratt & Whitney also developed a model for Laser Powder Deposition of titanium and this model has been extended to model the cold spray process for titanium [4].

The fig.1.7 shows the value stream analysis for making a component. The Value Stream Analysis shows that by using the cold spray process reduction in cost can be achieved in the following areas:-

1) Material input
2) Reduction in finishing time
3) Reduction in rework time
4) Reduction in the cost of mould preparation and melt pouring
5) Increase in material utilization because the deposition efficiency in cold spraying is 60 to 90% [4].
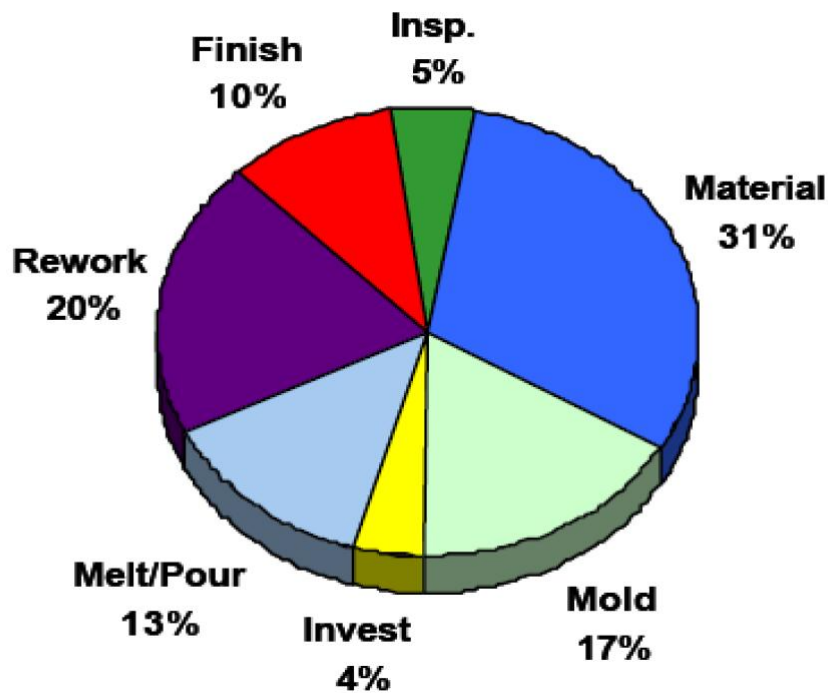
Figure 1.7: Value stream analysis

The Value Stream results showed that 70% of the value stream could be achieved if rework and finishing were reduced by 75%, material input reduced by 50%, and mould, casting cost and melt/pour cost reduced by 70%. These estimated figures show that it is advantageous to use a cold spray process because of a reduction in the manufacturing cost of components. [4] For example, in the production of large ring rolling and billets made from titanium alloys. Titanium is a very hard material and it can take many days to machine each piece. The process wears out many of the cutting tools and more than 90% of the material is machined away in getting the final product. This can cost more than $ 1 million dollars apiece. Even in large scale production there can be a long lead time because of the limited availability of titanium, the processing capacity and the considerable time to convert stock material into final product, so the cold spray process is used to manufacture near net shapes by depositing titanium alloys [19].

1.4.2 Equipment Used In Cold Spraying

A block diagram of cold spray equipment with a powder heater installed is shown in fig.1.8
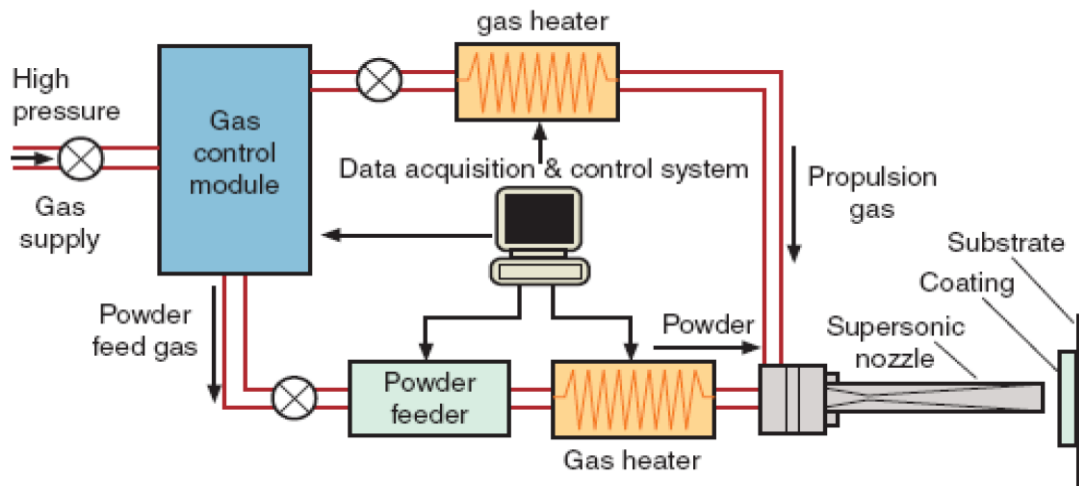
Figure 1.8: The block diagram of cold spraying system

Figure 1.9: The cold spray system in ASB Industry, Inc [4]

The main parts of the cold spray system involves

1) A gas control module which contains the working gases such as helium, nitrogen, argon, and mixes of these gases and which enter the nozzle at higher pressure.

2) A data acquisition and control system for controlling the gas pressure from the compressor, the powder feed rate into the nozzle and the gas heater that maintains the proper temperature of the gas.[20]

3) A powder feeder which delivers powder in a continuous flow at a mass flow rate of 5 to 10 kg/h to make a uniform coating and improve reliability for measuring deposition efficiency. The powder feeders currently available with features like low maintenance, uniform and accurate powder feeding, low powder wastage, minimal pulsing and easy cleaning.[16]

4) A gas heater is used to heat the gas up to a temperature ranging from 300° to 650°C before it enters the nozzle. Heating the gas eventually increases the powder particles temperature and velocity and hence ensures plastic deformation after they strike a substrate. However the gas temperature at the inlet of the nozzle is below melting point which means particles do not melt during the process.[21]

5) In the coating process, nozzle is the main component for depositing solid-state particles. In the cold spray process, a convergent-divergent De Laval type nozzle is used to accelerate the particles at supersonic speed by the gas flow. After leaving the nozzle at high velocity, the particles impinge on the work piece and undergo plastic deformation because of collision and bonding with the work piece surface and other particles to make a coating. Studies show [22] that better injection through the nozzle gives the following benefits in coating formation:-

   a) It enables the use of an increased gas temperature for the cold spray process.

b) The dwell time of the sprayed particles can be increased before they enter the convergent divergent nozzle and heat the particle.

c) More powder gas flow can be used without clogging the nozzle hence increasing the effective temperature of propellant gas [22].

1.4.3 Factors Affecting the Cold Spray Process

Recent research on the cold spray process shows that successful coating formation on a substrate depends upon the velocity of the particles exiting the nozzle and striking the surface of work piece. The velocity further depends upon factors such as gas temperature, gas pressure, type of gas used [23], the size of the particles used for spraying and the nozzle design which includes the throat diameter, inlet diameter, outlet diameter, convergent and divergent length of the nozzle [24].

1.4.3.1 Effect of Gas Temperature

Previous studies have found that if the temperature of the carrier gas is increased then it directly affects the velocity of the particles [21] [22] [25] and it also results in higher deposition efficiency of the particles on the substrate. Compressed gas enters the convergent divergent nozzle with an inlet pressure of around 27-35 bar to get the supersonic velocity. The solid powder particles are introduced in the nozzle upstream (convergent portion) and are accelerated by the rapidly expanding gas in the divergent part of the nozzle. The carrier gas is often preheated to get high gas flow velocities through the nozzle. In the cold spray process the gas is first heated to a temperature ranging from 300 K to 900 K. Particles when introduced into a hot gas stream, are in contact with the gas for a shorter time, so that when the gas expands in the divergent part its temperature decreases. In this process the temperature of the particles remains below their melting temperature [26]. The main gases which are used for cold spraying are helium and nitrogen because of their lower molecular weight and larger specific heat ratio.
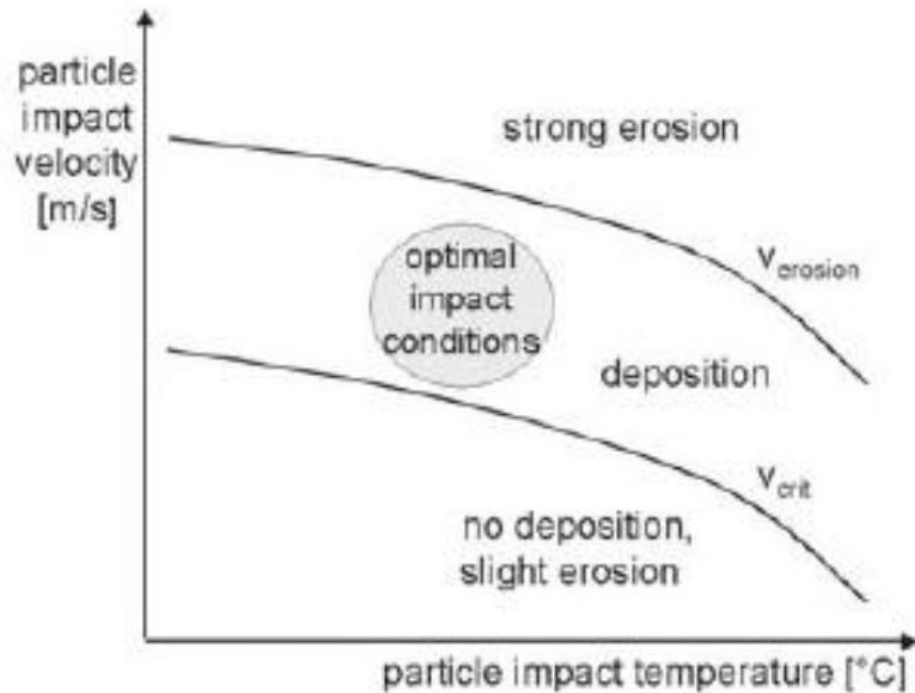
Figure 1.10: Critical particle impact velocity as a function of particle temperature with optimum impact conditions [25]

The main consideration arising from increasing the temperature of the gas is the robustness of the nozzle material, which results in getting limited particle velocity and temperature. The German company CGT commercially manufactured a tungsten carbide MOC-nozzle which can spray copper particles at 600° C at a pressure of 30 bars without plugging and erosion of the nozzle material [25]. The main advantage of a high impact temperature is that it decreases the critical velocity of the spray material because of thermal softening. The Figure 1.10 shows the two lines which indicate the critical velocity and erosion velocities. Both are temperature dependent [25].

The deposition efficiency also depends upon the temperature of the carrier gas. It was found that when nitrogen is used to spray titanium particles the critical temperature is 155 °C, below this temperature no particle deposition took place.

When the temperature was further increased from this critical temperature, the deposition efficiency also increased rapidly, especially when the temperature of nitrogen exceeded 215 °C.

1.4.3.2 Effect of Gas Pressure

In an experiment performed by M. Fukumoto *et al* [27] the effect of the gas inlet pressure on the deposition efficiency was investigated and the results showed that deposition efficiency increases with increase in the gas pressure.

Cold spray systems are subdivided into two categories high pressure systems and low pressure systems on the basis of gas pressure. Fig.1.11 shows the higher pressure system. A separate gas compressor is required in these systems and gases such as helium is used in this system because of its low molecular weight to achieve very high particle velocity.Fig.1.12 shows the lower pressure system. In a low pressure system a powder stream is injected into the nozzle at the point where gas has expanded to low pressure. Since no pressurized feeder is required in this system, it is often used in portable cold spray systems.
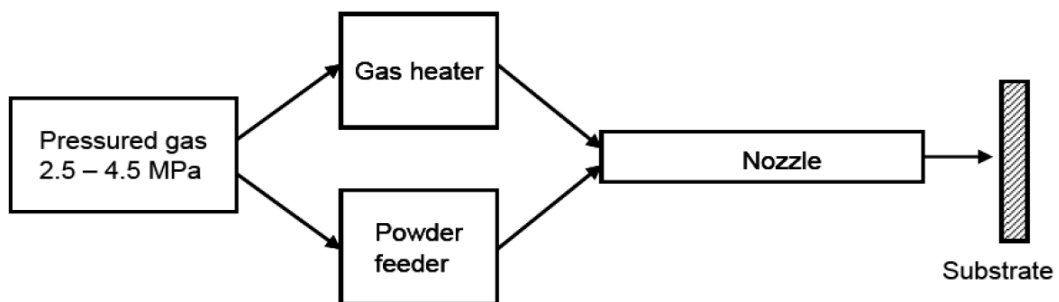
Figure 1.11: High pressure system
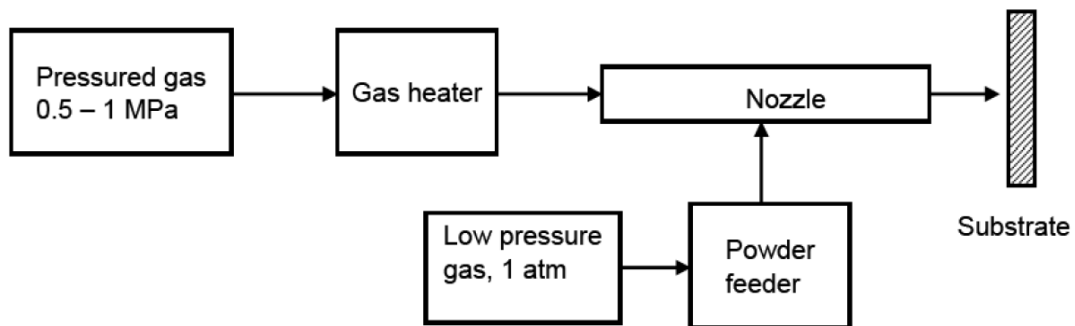
Figure 1.12: Low pressure system

1.4.3.3   The Effect of the Type of Gas

In cold spray processes the type of gas used to spray powder particles plays an important role in the acceleration of particles. In most cases nitrogen, helium, air or the mixture of air and helium or air and nitrogen are used as carrier gasses because of their lower molecular weight [28].

Initially experiments using helium as a carrier gas were very successful in achieving high adhesion and corrosion resistant coatings. Cold spray process parameters were also developed with nitrogen to reduce the costs while maintaining satisfactory coating performance [29]. In one-dimensional flow theory the Mach number at the throat is assumed to be unity and the velocity of gas can be calculated from:

$$V = \overline{\gamma R T}$$

Where γ is specific heat ratio, T is temperature of gas and R is the specific gas constant (the universal gas constant is divided by the gas molecular weight). The above equation shows why it is often found that helium makes a better carrier gas for cold spraying. It has a smaller molecular weight and higher specific heat ratio [23]. The specific heat ratios of nitrogen and helium are 1.4 and 1.66 respectively. The specific gas constants for nitrogen and helium are 296.8 J/Kg K and 2,077 J/Kg K respectively. According to the above equation the velocity of nitrogen will be lower than the velocity of helium, and when the temperature of the gas is increased

the gas velocity increases. Subsequently the particle velocity also increases. The drag force on particles increases when gas pressure is increased because higher gas pressure increases the density of the gas [24].

1.4.3.4   The Effect of Particle Size

Previous study shows that the powder particles used for spraying have a wide size distribution range [28][29][30]. The powder is fed into a gas stream flowing through the nozzle. The acceleration of each particle depends upon its size. Particles cannot make a coating if they are very small in size or light in weight, because then they will follow the flow where as if the powder particles are very heavy or large in size they will not get the kinetic energy from the carrier gas to strike the substrate [30]. Small particles achieve high acceleration and large particles achieve less acceleration. For making a successful powder deposit only the particles with a velocity greater than a critical velocity can contribute to the coating. Hence it is very important to consider the particle size before carrying out cold spraying. The particles size distribution can be expressed by the following Rosin-Rammler formula:

$$Y_d = e^{-\frac{d}{d}^n}$$

Where Y_d is the mass fraction and 'n' is the size distribution   At high temperatures more plastic deformation occurs in particles when they strike a substrate and this improves deposition efficiency [31]. A previous study shows that the particle temperature reaches maximum value when the diameter of the particle is 10μm. This behaviour is determined by the particle and gas phase heat transfer. There is a maximum temperature profile for the smaller particles because the heat transfer rate is faster for smaller particles. In larger particles, the temperature increases slowly [32].

1.4.4 Cold Spray Nozzle

The first practical use of a convergent divergent nozzle was in the 1800s by the Swedish engineer Carl G. P. De Laval. He designed a steam turbine which incorporated a supersonic expansion nozzle upstream of the turbine blades. Initially

some nozzles were convergent in shape and other designs the nozzle was nothing more than an orifice. In 1882, de Laval added a divergent section to the original convergent shape. By changing the nozzle design his steam turbines began to run at a very high speed. Subsequently his design was demonstrated at the World Columbian Exposition in Chicago in 1893. It was through this steam turbine design that de Laval made a lasting contribution to the advancement of compressible flow [33].
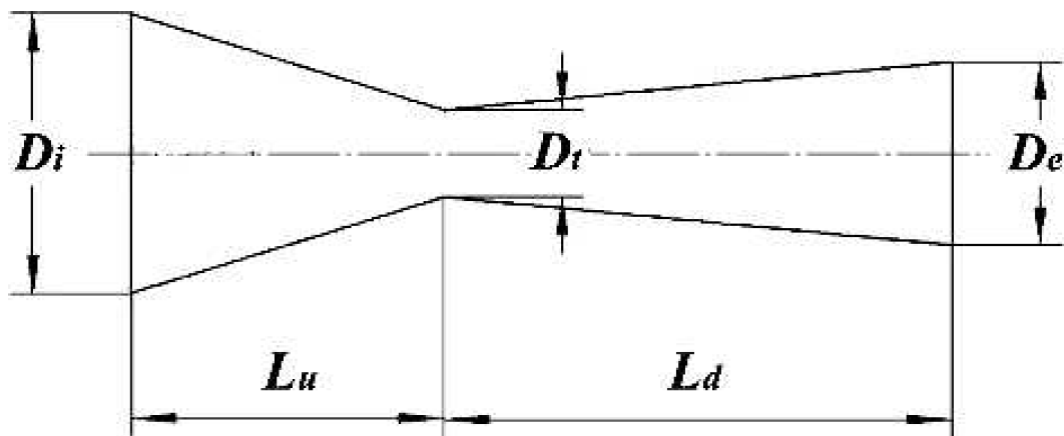
Figure 1.13: Diagram of de-Laval nozzle

Where Dt is the diameter of nozzle throat Di & De are the inlet and outlet diameter of the nozzle and Lu & Ld are convergent and divergent length of the nozzle.

1.4.4.1   Reason for Using a De-Laval Nozzle

In cold spray, a high particle velocity can be achieved by using high propellant gas pressure and De Laval nozzle designs. Before the gas enters the converging part of the nozzle it is preheated to attain a high velocity at the throat [17].

The reason behind using the convergent divergent De Laval nozzle is to get supersonic velocity, which is possible because of its design. The Area-Velocity relation for flow through the nozzle is given by

$$\frac{dA}{dx} = \frac{A(M^2 - 1)}{u} \frac{du}{dx}$$

1. For subsonic flow i.e. M<1, we have $(M^2\text{-}1)$ <0. Hence if dA/dx <0, then du/dx >0, and if dA/dx >0, then du/dx <0. Thus, the velocity of a subsonic flow increases if it passes through a converging duct, and decreases as it passes through a diverging one.
2. For supersonic flow, we have $(M^2 - 1)$ >0, and the situation is reversed; when flow passes through the converging part the velocity decreases and increases when flow passes through the diverging part.
3. For sonic flow, i.e. M =1, we have dA/dx =0, which corresponds to a maximum or a minimum in the area distribution. However, only the minimum area solution is the physically realistic solution [34].

Previous studies [35] have found that the critical velocity of most materials is more than 700 m/s, which shows the importance of supersonic flow for carrying these particles. To optimize the nozzle shape the one-dimensional flow model has to be analytically studied knowing the given gas condition, powder size and nozzle dimensions. It is necessary to know the minimum particle velocity for designing the cold spray nozzle so that a particular powder material bonds well to a substrate. It is found that gas density and nozzle length play an important part in accelerating the particle to a velocity close to the gas velocity [45]. The Fig.1.14 shows the critical velocities of different materials used for cold spraying.
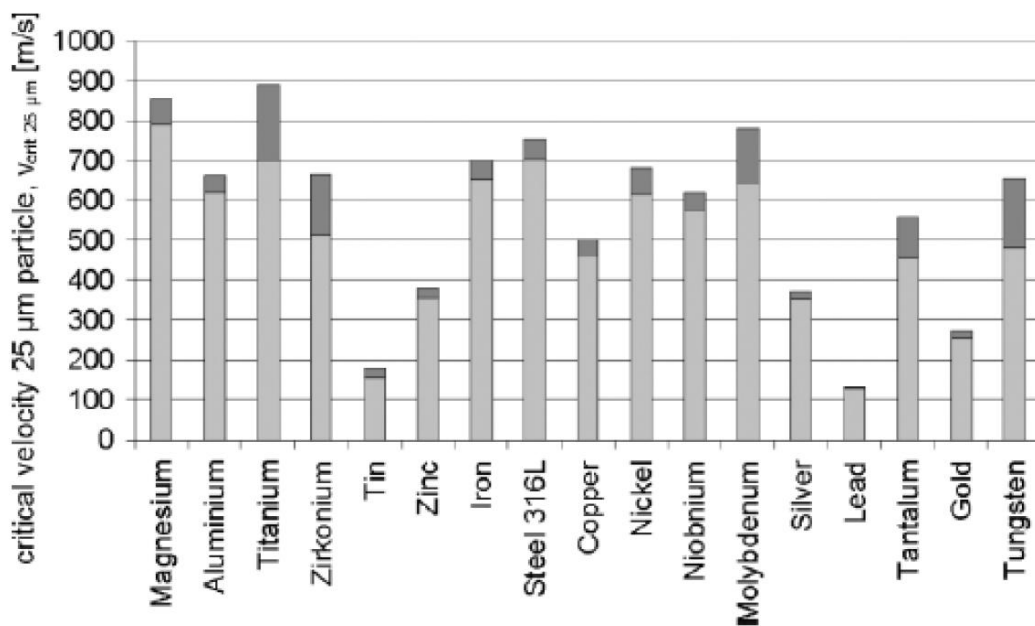
Figure 1.14: Calculated critical velocities for various spray materials [17]

By using computational codes like CFD the nozzle shape can be improved or evaluated. High velocity can be achieved by having a properly shaped nozzle and if the velocity is increased from the critical velocity it not only affects the deposition efficiency but also the coating quality [17].

1.4.4.2   Optimization of Nozzle Design

One-dimensional isentropic flow analysis has been used to show the general and specific nozzle geometry and pressure ratio required to generate a shock-free supersonic flow. B. Jodoin shows that nozzle geometry and pressure ratios are the only factors to consider when designing cold spray nozzles operating at a specific Mach nozzle. [35] By improving the nozzle design high particle velocity can be achieved which leads to high deposition efficiency. To increase the velocity of particles, gas dynamic models were used. In one of the examples it was found that if the length of the nozzle was increased from 83 mm to 211 mm, and using nitrogen as a carrier gas with 12 μm copper particles the maximum velocity can be increased from 553 m/s to 742 m/s. This is an increase in 33% in particle velocity and 80%

increase in deposition efficiency [36]. The strong bond between the particle and substrate depends upon the contact pressure between the particle and substrate which is only achieved by the high kinetic energy of the particles [37][38].

From previous simulation results obtained by assuming one-dimensional isentropic flow indicates that particle velocity can be varied by changing the expansion ratio of the nozzle [25]. An optimal expansion ratio for particle acceleration of about 4 and 6.25 for nozzles with divergent lengths of 100 and 40 mm respectively were found [51]. However these optimal values may not be accurate because changes in the nozzle exit diameter in simulations were not precise. Previous studies show that nozzle inlet diameter and convergent length has very little influence on particle velocity so more attention in previous research has been paid to the divergent length, the throat diameter and the exit diameter of the nozzle[39].

1.4.5 Challenges

Based on the above review, following the major technical challenges are found in cold spray system.

- Size distribution of particles to be sprayed.
- Position of injection of particles.
- Injecting pressure.
- Types of carrier gas to be used.
- Temperature of carrier gas to be used.
- Standoff distance.
- Nozzle size.

1.4.6 Objective

Most of the references available in open literature have performed experimental studies to understand the various factors affecting cold thermal spraying process. However experimental studies in controlled environment are often expensive and difficult to perform. However computational studies using computational fluid

dynamics (CFD) offer a more cost effective alternative to experimental studies. Very few CFD studies have been reported in open literature [33] [34] [35].

The main objective of this study was to develop a methodology to study performance parameters of cold spray technique using CFD. Commercial CFD software ANSYS FLUENT 13 was used in this study.

Initially the efficacy of using CFD for the thermal spray technique was established on a 2D geometry. Various grid densities; flow parameters like turbulence models; boundary conditions; numerical parameters like solver settings, pressure velocity coupling were evaluated on this geometry and validated against experimental and numerical studies available in open literature. Following this parametric studies of particle size distribution, position of injected particles, injection pressure, carrier gas temperature and carrier gas type was studied. All the studies were performed on a 2D geometry. The effect of coupled and uncoupled approach, injection pressure and particle size distribution was also studied on a 3D geometry. The effectiveness of these parameters were evaluated by estimating velocity distribution of the particles at the exit and comparing this parameters with the critical velocity to good surface adhesion.

Chapter 2

Numerical Methodology

2.1 Geometry
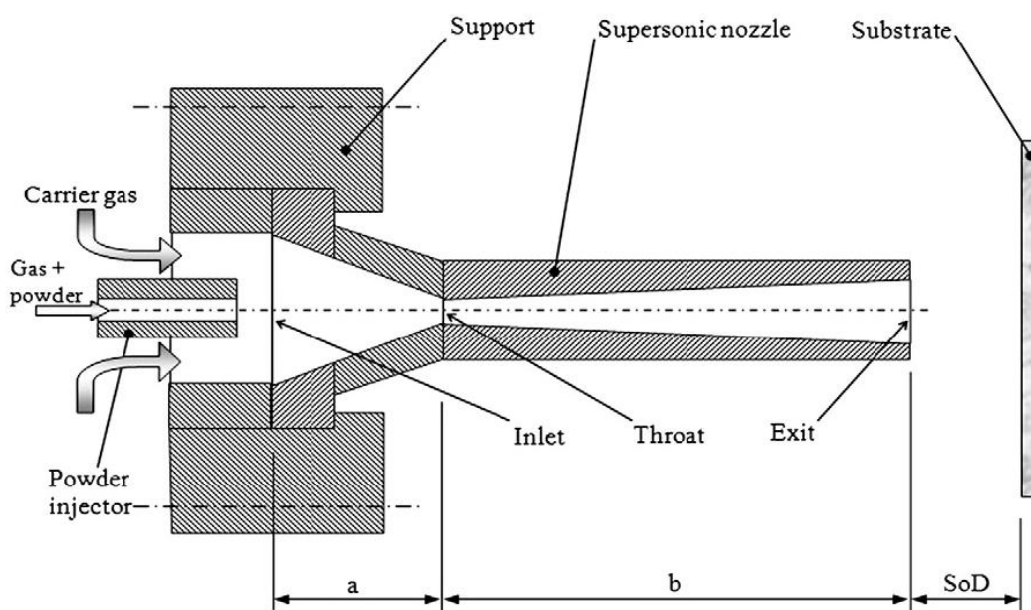
Figure 2.1: Schematic of the Nozzle

A schematic diagram of the cold spray system is shown in fig.2.1. The spraying gun of the system comprises a supersonic converging– diverging nozzle and a powder injector. The injector outlet is located near the convergent part of the nozzle because it is a high pressure system. In low pressure system the injector outlet is located after the throat(low pressure area) of the nozzle. A pressurized carrier gas fed through a number of ports enters the nozzle inlet zone of length a. At the same time, a mixture of gas and powder is delivered from a powder feeder to the powder injector shown in the figure. The carrier gas will therefore expand up to atmospheric pressure and accelerate throughout the main nozzle total length (a+b), giving sonic velocity at

the throat and supersonic velocity at the exit. Particles are dragged by the carrier gas up to high velocity magnitudes, resulting in severe plastic deformation processes upon impact with a solid substrate positioned at the distance SoD (Standoff Distance). As a consequence, bonding with the substrate can occur and the coating process can be initiated. The substrate is connected to a CNC table which moves the substrate in X and Y directions at an imposed speed.

2.2 Introduction to CFD

Euler-Lagrange (Two way coupling) Discrete Phase Modeling (DPM) algorithm implemented in Fluent 13 was used in this study. In this approach the fluid phase is treated as a continuum by solving the Navier-Stokes equations, while the dispersed phase is solved by tracking a large number of particles through the calculated flow field. The dispersed phase can exchange momentum, mass, and energy with the fluid phase. The physical properties of all fluid flow are governed by the following three fundamental equations:

Continuity equation The general continuity equation is written as follows:

$$\frac{\partial \rho}{\partial t} + \frac{\partial}{\partial x_i}\left(\rho u_i\right) = 0 \tag{1}$$

Here ρ is the density

Momentum equations The momentum equation that is solved in this study is:

$$\frac{\partial}{\partial t}\left(\rho u_i\right) + \frac{\partial}{\partial x_j}\left(\rho u_i u_j\right) = -\frac{\partial p}{\partial x_i} + \frac{\partial \tau_{ij}}{\partial x_j} + \rho g_i + F_i \tag{2}$$

Where p is static pressure, τij is the stress tensor, ρgi is the body force due to gravity and Fi is the external body force. As we are dealing with supersonic flow, ρgi is very small compared to external body forces, so it is neglected in this study.

Energy equation The energy equation is written as follows:

$$\frac{\partial}{\partial t}\left(\rho E\right) + \frac{\partial}{\partial x_i}\left(u_i\left(\rho E + P\right)\right) = \frac{\partial}{\partial x_i}\left(k\frac{\partial T}{\partial x_i} - \sum_j h_j J_j + u_j \tau_{ij}\right) + S_h \qquad (3)$$

Where E is the total energy per unit mass, k is the conductivity, Jj is the diffusion flux of species j and Sh is the source term which refers to any heat source.

These basic principles for a flowing fluid can be written mathematically in the form of partial differential equations. Basically Computational Fluid Dynamics (CFD) replaces the governing differential equations with numbers to represent the fluid flow, and these numbers are put in three-dimensional space with a time interval to get the desired flow field in numerical form. The final outcome of the CFD is a group of numbers in closed form which represent a flow field analytically. The application of CFD for more complex and sophisticated cases depends mostly upon the computational resources like storage capacity and computational speed (RAM) [40].

2.3 Introduction to AnsysFLUENT

AnsysFluent is one of the major commercially available computational fluid dynamics (CFD) software. For doing Computational Fluid Dynamics AnsysFLUENT uses computer as a tool for analyzing and designing models. Fluent is computer software used for making models of flowing fluid and heat transfer. In fluent geometry of very complex models can be formed by using different type of meshes for solving the problems related to fluid flow. It also allows the mesh refining or coarsening depends on the solution required [40].

2.4 Numerical Procedure

To attain supersonic velocity of the gas stream, it is necessary to construct the geometry of a Convergent-divergent de-Laval nozzle [41]. ICEM CFD is used to create the geometry and mesh used in this study. The simulation can be used to determine the various flow parameters like the pressure and temperature of the gas phase, velocity of the copper particles used in this spray, etc. It can also be used to

determine the optimum operating parameters needed for achieve a good quality cold spray.

For analyzing the flow parameters, 3D model & 2D axisymmetric model of the nozzle was created, because 3D model will predict the turbulence accurately. The reasons for making axisymmetric were:

- It reduces the computational effort required to solve the problem, and therefore it takes less time to get a converged solution.

- Flow field and geometry were symmetrical.

- Zero normal velocity at the plane of symmetry.

- Zero normal gradients of all variables at plane of symmetry.

The plane of symmetry was specified as the axis in boundary specifications and the nozzle model was defined such that flow, pressure gradient and temperature were zero along this specified edge of the domain.

Using an axisymmetric model reduces computational effort but it does not affect the outcome of the simulation. Y. Li *et al*. [42] who investigated both the axisymmetric nozzle and two-dimensional full nozzle, found good agreement with the experimental results.

2.4.1 Model Parameters

The nozzle for cold spraying of copper particles was simulated by commercial code AnsysFLUENT 13 using the 2D&3D double precision density solver to see the effects of the different parameters on the velocity of the copper particles, and how changing different parameters like temperature, pressure and size of the particles affects their velocity. From the literature[42], it was found that the velocity of the particles could be influenced by the nozzle expansion ratio (i.e. ratio of area of exit of nozzle to the area of throat).

The coupled implicit density-based solver along with the Green-Gauss Cell Based gradient method was used to simulate the flow field inside the nozzle. The flow, turbulent kinetic energy, and turbulent dissipation rate were modelled using second order upwind accuracy.

2.4.2 Second Order Scheme

In the second order scheme, the values of cells are computed by using a multidimensional linear reconstruction approach. This approach was used for obtaining higher order accuracy and is achieved at cell faces by a Taylor series expansion of the cell centred solution of the cell centroid. The face value Øf is computed using the following expression:

$$\emptyset f = \emptyset + \nabla\emptyset.\Delta s \tag{4}$$

Where $\emptyset$ and $\nabla\emptyset$ are the cell centred values and their gradient in the upstream cell, and Δs is the displacement vector from the upstream cell centroid to the face centroid. This formulation requires the determination of the gradient $\nabla\emptyset$ in each cell. This gradient is computed by using the divergence theorem, which in discrete form is written as:

$$\Delta\emptyset = \frac{1}{V} \sum_{f}^{N_{faces}} \emptyset_f A \tag{5}$$

Here the face values $\emptyset f$ are computed by averaging $\emptyset$ from the two cells adjacent to the face. Finally, the gradient $\nabla\emptyset$ is limited so that no new maxima or minima are introduced.

2.5 Turbulence Modelling

The fluid flowing through the nozzle had a very high Reynolds number (more than 50,000), so the flow can be said to be fully turbulent. Different turbulence models adopt different approaches for tackling turbulence but choosing the right model

ensures the accuracy of the final solution. Modelling turbulence is very complex and a highly technical field, and the selection of a turbulence model depends on factors including accuracy, computational time, resources available, and application.

In this thesis two types of turbulence models were used.

1) **Realizable k-ε turbulence model** for two dimensional analysis and
2) **DES turbulence model** for three dimensional analysis.

2.5.1 Realizable k-ε Model

The realizable k-ε model is a relatively recent development and differs from the standard k-ε model in two important ways:

- The realizable k-ε model contains a new formulation for the turbulent viscosity.
- A new transport equation for the dissipation rate, ε has been derived from an exact equation for the transport of the mean-square vorticity fluctuation.

The term "realizable" means that the model satisfies certain mathematical constraints on the Reynolds stresses, consistent with the physics of turbulent flows. The standard k-ε model or its variants like the RNG k-ε are realizable.

An immediate benefit of the realizable k-ε model is that it more accurately predicts the spreading rate of both planar and round jets. It is also likely to provide superior performance for flows involving rotation, boundary layers under strong adverse pressure gradients, separation, and recirculation.

To understand the mathematics behind the realizable k-ε model, consider combining the Boussinesq relationship and the eddy viscosity definition to obtain the following expression for the normal Reynolds stress in an incompressible strained mean flow:

$$\overline{u}^2 = \frac{2}{3}k - 2\vartheta_t \frac{\partial U}{\partial x} \tag{6}$$

Using $\vartheta_t \equiv \frac{\mu_t}{\rho}$ one obtains the result that the normal stress, $\overline{u}^2$, which by definition is a positive quantity, becomes negative, i.e., "non-realizable", when the strain is large enough to satisfy

$$\frac{k}{\varepsilon}\frac{\partial U}{\partial x} > \frac{1}{3C_\mu} \approx 3.7 \tag{7}$$

Both the realizable and RNG k-ε models have shown substantial improvements over the standard k-ε model where the flow features include strong streamline curvature, vortices, and rotation. Studies have shown that the realizable model provides superior performance compared to other variants of k-ε model for separated flows and flows with complex secondary flow features.

One of the weaknesses of the standard k-ε model or other traditional k-ε models lies with the modeled equation for the dissipation rate (ε). The well-known round-jet anomaly is considered to be mainly due to the modeled dissipation equation. The realizable k-ε was intended to address these deficiencies of traditional k-ε models by adopting the following:

- Eddy-viscosity formula involving a variable C_μ originally proposed by Reynolds.
- dissipation (ε) is modelled based on the dynamic equation of the mean-square vorticity fluctuation.

2.5.1.1 Transport Equations for the Realizable k-ε Model

The modeled transport equations for k and ε in the realizable k-ε model are

$$\frac{\partial}{\partial t} \rho k + \frac{\partial}{\partial x_j} \rho k u_j = \frac{\partial}{\partial x_j} \left[\mu + \frac{\mu_t}{\sigma_k} \right] \frac{\partial}{\partial x_j} + G_k + G_b - \rho\varepsilon - Y_M + S_K \tag{8}$$

And

$$\frac{\partial}{\partial t}\left(\rho\epsilon\right) + \frac{\partial}{\partial x_j}\left(\rho\epsilon u_j\right) = \frac{\partial}{\partial x_j}\left[\left(\mu + \frac{\mu_t}{\sigma_\epsilon}\right)\frac{\partial\epsilon}{\partial x_j}\right] + \rho C_1 S_\epsilon - \rho C_2 \frac{\epsilon^2}{K + \sqrt{\vartheta\epsilon}}$$

$$+ C_{1\epsilon}\frac{\epsilon}{k}C_{3\epsilon} \tag{9}$$

Where

$$C_1 = max\left[0.43, \frac{n}{n+5}\right], \qquad n = S\frac{k}{\epsilon}, \qquad S = \sqrt{2s_{ij}s_{ij}}$$

In these equations , G_k represents the generation of turbulent kinetic energy due to the velocity gradients. G_b is the generation of turbulent kinetic energy due to buoyancy. Y_m represents the contribution of the fluctuating dilatation in compressible turbulence to the overall dissipation rate. C_1 & C_2 are constants. σ_k and σ_ε are the turbulent prandtl numbers for k and ϵ respectively. S_k and S_ϵ user defined source terms. The k equation is same as that in the standard k-ε model and the RNG k-ε model, except for the model constants. However, the form of the ε equation is quite different from those in the standard and RNG-based k-ε models. One of the noteworthy features is that production term in the ε equation does not involve the production of k; i.e. it does not contain the same G_k term as the other k-ε models.

2.5.2 Detached Eddy Simulation (DES) Model

In the DES approach, the unsteady RANS models are employed in the boundary layer, while the LES treatment is applied to the separated regions. The LES region is normally associated with the core turbulent region where large unsteady turbulence scales play a dominant role. In this region, the DES models recover LES-like sub grid models. In the near-wall region, the respective RANS models are recovered.

DES models have been specifically designed to address high Reynolds number wall bounded flows, where the cost of a near-wall resolving Large Eddy Simulation would be prohibitive. The difference with the LES model is that it relies only on the

required resolution in the boundary layers. The application of DES, however, may still require significant CPU resources and therefore, as a general guideline, it is recommended that the conventional turbulence models employing the Reynolds-averaged approach be used for practical calculations.

The DES models, often referred to as the hybrid LES/RANS models combine RANS modeling with LES for applications such as high-Re external aerodynamics simulations. In ANSYS FLUENT, the DES model is based on the one-equation Spalart-Allmaras model, the realizable k-ϵ model, and the SST k-ω model. The computational costs, when using the DES models, is less than LES computational costs, but greater than RANS.

2.5.2.1 Spalart-Allmaras Based DES Model

The standard Spalart-Allmaras model uses the distance to the closest wall as the definition for the length scale d, which plays a major role in determining the level of production and destruction of turbulent viscosity. The DES model, as proposed by Shur et al. replaces d everywhere with a new length scale d, defined as

$$d \ = \ \min(d, C_{des}\Delta) \tag{10}$$

where the grid spacing, Δ, is based on the largest grid space in the x, y, or z directions forming the computational cell. The empirical constant C_des has a value of 0.65.

For a typical RANS grid with a high aspect ratio in the boundary layer, and where the wall-parallel grid spacing usually exceeds δ, where δ is the size of the boundary layer, equation (10) will ensure that the DES model is in the RANS mode for the entire boundary layer. However, in case of an ambiguous grid definition, where Δ $<< \delta$, the DES limiter can activate the LES mode inside the boundary layer, where the grid is not fine enough to sustain resolved turbulence. Therefore, a new formulation of DES is available in ANSYS FLUENT to preserve the RANS mode

throughout the boundary layer. This is known as the delayed option or DDES for delayed DES.

The DES length scale d is re-defined according to:

$$d = d - f_d \max(0, d - C_{des}\Delta) \tag{11}$$

Where f_d is given by

$$F_d = 1 - \tanh\ (8r_d)^3 \tag{12}$$

2.5.2.2 Realizable k-ε based DES model

This DES model is similar to the Realizable k-ε model with the exception of the dissipation term in the k equation. In the DES model, the Realizable k-ε RANS dissipation term is modified such that:

$$Y_k = \frac{\rho k^{\frac{3}{2}}}{l_{des}} \tag{13}$$

Where

$$l_{des} = \min\ l_{rke}, l_{les} \tag{14}$$

$$l_{les} = C_{des}\Delta \tag{15}$$

Where C_{des} is a calibration constant used in the DES model and has a value of 0.61 and Δ is the maximum local grid spacing $(\Delta x, \Delta y, \Delta z)$.

For the case where $l_{des} = l_{rke}$, you will obtain an expression for the dissipation of the k formulation for the Realizable k-ε model : $Y_k = \rho\varepsilon$ Similarly to the Spalart-Allmaras model, the delayed concept can be applied as well to the Realizable DES model to preserve the RANS mode throughout the boundary layer. The DES length l_{des} is redefined such that

$$l_{des} = l_{rke} - f_d \max(0, l_{rke} - C_{des}\Delta) \qquad (16)$$

2.5.2.3 SST k-ω Based DES Model

The dissipation term of the turbulent kinetic energy is modified for the DES turbulence model as

$$Y_k = \rho \beta^* k \omega F_{DES} \qquad (17)$$

Where F_{DES} expressed as

$$F_{DES} = max\left[\frac{L_t}{C_{des}\Delta}, 1\right] \qquad (18)$$

where C_{des} is a calibration constant used in the DES model and has a value of 0.61, Δ is the maximum local grid spacing ($\Delta x, \Delta y, \Delta z$).

The turbulent length scale is the parameter that defines this RANS model:

$$L_t = \frac{\overline{k}}{\beta^* \omega} \qquad (19)$$

The DES-SST model also offers the option to "protect" the boundary layer from the limiter (delayed option). This is achieved with the help of the zonal formulation of the SST model. F_{DES} is modified according to

$$F_{DES} = max\left[\frac{L_t}{C_{des}\Delta}(1 - F_{SST}), 1\right] \qquad (20)$$

With $F_{SST} = 0, F_1, F_2,$ where F_1 and F_2 are the blending functions of the SST model.

2.6. Discrete Phase Modelling

AnsysFluent provides a model that is specially developed for spray simulations, or more general suspended particle trajectory simulations. This is the Discrete Phase Model (DPM) and it is based on the so-called Euler-Lagrange method. In the computational domain there are two separate phases present, namely the continuous and the discrete phase (particles). The transport equations from the previous section are solved for the continuous phase only and the motion of particles is dealt with particle trajectory calculations. Through an iterative solution procedure the mass, momentum and energy interaction between both phases can be realized. Some important aspects of the DPM model are presented in this section.

2.6.1 The Euler-Lagrange Approach

The discrete phase modelling follows the Euler-Lagrange approach. In this approach the fluid phase is treated as a continuum by solving the Navier-Stokes equations, while the dispersed phase is solved by tracking a large number of particles through the calculated flow field. The dispersed phase can exchange momentum, mass, and energy with the fluid phase.

A fundamental assumption made in this model is that the dispersed second phase occupies a low volume fraction, even though high mass loading ($m_{particles} \geq m_{fluid}$) is acceptable. The particle or droplet trajectories are computed individually at specified intervals during the fluid phase calculation. This makes the model appropriate for the modeling of spray dryers, coal and liquid fuel combustion, and some particle-laden flows.

2.6.2 Particle Motion

The trajectory calculation of a discrete phase particle is done by integrating the force balance on the particle, which is written in a Lagrangian reference frame. This force balance equates the particle inertia with the forces acting on the particle, and can be written (for the x direction in Cartesian coordinates) as

$$\frac{du_p}{dt} = F_D \left(u - u_p \right) + \frac{g_x(\rho_p - \rho)}{\rho_p} + F_x \tag{21}$$

where the left hand term is the acceleration of the particle, F_x is an additional acceleration due to external force field and the term with F_D is the drag force on the particle. F_D is defined as:

$$F_D = \frac{18\mu}{\rho_p d_p^2} \frac{C_D R_e}{24} \tag{22}$$

where u is the fluid phase velocity, u_p is the particle velocity, μ is the molecular viscosity of the fluid, ρ is the fluid density, ρ_p is the density of the particle, d_p is the particle diameter and R_e is the relative Reynolds number.

2.6.3 Turbulent Dispersion of Particles

The dispersion of particles due to turbulence in the fluid phase can be predicted using the stochastic tracking model or the particle cloud model. The stochastic tracking (random walk) model includes the effect of instantaneous turbulent velocity fluctuations on the particle trajectories through the use of stochastic methods. The particle cloud model tracks the statistical evolution of a cloud of particles about a mean trajectory. The concentration of particles within the cloud is represented by a Gaussian probability density function (PDF) about the mean trajectory. For stochastic tracking a model is available to account for the generation or dissipation of turbulence in the continuous phase. Turbulent dispersion of particles cannot be included if the Spalart-Allmaras turbulence model is used.

2.6.3.1 Stochastic Tracking

When the flow is turbulent, AnsysFLUENT will predict the trajectories of particles using the mean fluid phase velocity, $\overline{u}$, and the fluctuating velocity u'

$$u = \overline{u} + u' \tag{23}$$

In the stochastic tracking approach, AnsysFLUENT predicts the turbulent dispersion of particles by integrating the trajectory equations for individual particles, using the instantaneous fluid velocity, $\bar{u} + u'(t)$, along the particle path during the integration. By computing the trajectory in this manner for a sufficient number of representative particles (termed the "number of tries"), the random effects of turbulence on the particle dispersion can be included.

ANSYS FLUENT uses a stochastic method (random walk model) to determine the instantaneous gas velocity. In the discrete random walk (DRW) model, the fluctuating velocity components are discrete piecewise constant functions of time. Their random value is kept constant over an interval of time given by the characteristic lifetime of the eddies.

The DRW model may give nonphysical results in strongly nonhomogeneous diffusion-dominated flows, where small particles should become uniformly distributed. Instead, the DRW will show a tendency for such particles to concentrate in low-turbulence regions of the flow.

2.6.3.2 Particle Cloud Tracking

In particle cloud tracking, the turbulent dispersion of particles about a mean trajectory is calculated using statistical methods. The concentration of particles about the mean trajectory is represented by a Gaussian probability density function (PDF) whose variance is based on the degree of particle dispersion due to turbulent fluctuations. The mean trajectory is obtained by solving the ensemble-averaged equations of motion for all particles represented by the cloud.

The cloud enters the domain either as a point source or with an initial diameter. The cloud expands due to turbulent dispersion as it is transported through the domain until it exits. As mentioned before, the distribution of particles in the cloud is defined by a probability density function (PDF) based on the position in the cloud relative to the cloud center. The value of the PDF represents the probability of finding particles represented by that cloud with residence time t.

2.6.4. Phase Coupling

While the discrete particle phase is always influenced by the continuous phase solution (one-way coupling). However, when the particle influences the flow characteristics of the continuous phase, then it is called two way coupling. In the one-way coupling case the continuous phase is solved first thereafter the particle trajectory calculation is performed. When two-way coupling is applied an iterative procedure is followed. Then, after the particle trajectory calculation the continuous flow field is solved again with updated source terms until convergence is reached.

2.6.4.1 Coupling Between the Discrete and Continuous Phases

As the trajectory of a particle is computed, ANSYS FLUENT keeps track of the heat, mass, and momentum gained or lost by the particle stream that follows that trajectory and these quantities can be incorporated in the subsequent continuous phase calculations as source terms. Thus, while the continuous phase always impacts the discrete phase, you can also incorporate the effect of the discrete phase trajectories on the continuum..
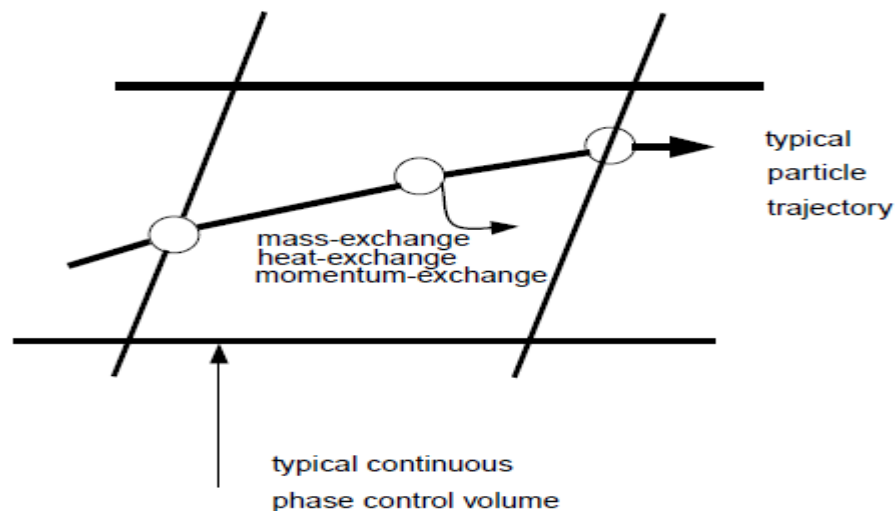
Figure 2.2: Heat, Mass, and Momentum Transfer Between the Discrete and Continuous Phases

This two-way coupling is accomplished by alternately solving the discrete and continuous phase equations until the solutions in both phases have stopped changing. This interphase exchange of heat, mass, and momentum from the particle to the continuous phase is depicted qualitatively in Fig.2.2. Note that no interchange terms are computed for particles defined as massless, where the discrete phase trajectories have no impact on the continuum

2.7 Flow Field

For the nozzle domain, the pressure inlet was used as the boundary condition at the nozzle inlet because of the better convergence rate compared to the mass flow inlet [54]. The inlet pressure for cold spraying was varied from 1.1 MPa to 3 MPa, and the Mach number at the throat was assumed to be unity due to choked flow condition.. The total temperature at the inlet boundary condition was 300K. The direction of the velocity vector was assumed to be normal to the direction of the boundary (outlet). The value of turbulence intensity was set at 10% and the turbulence viscosity ratio was assumes to be 10%. These values were validated by the cases in which these values were used for similar kinds of simulation or making flow fields [54] [56] [57]. Standard K-ε corrects these turbulence values according to the turbulence produced in the flow [23]. In order to achieve maximum velocity and to see the effect of changing parameters, like pressure and temperature, on the gas outlet velocity, air, nitrogen and helium were used to simulate the supersonic flow through a convergent-divergent nozzle.

The temperature of the gas for the inlet boundary condition was gradually increased from 300 K to 700 K. Pressure outlet was selected as the boundary condition at the nozzle outlet, with the static pressure equal to ambient pressure. Neighbouring cells were selected to obtain the direction of the velocity vector. The nozzle walls were considered to be adiabatic. As the heat transfer from the walls to the surrounding ambient was negligible the temperature of the walls was assumed to be 300 K.

2.8 Fluid Properties

Compressible fluids are those in which the fluid density changes with the high pressure gradients. For gases, varying the temperature changes the gas density. The fluid properties were changed from default settings to account for compressibility, and for changes in thermophysical properties like density with temperature. The ideal gas law was selected in the density drop-down list. The ideal gas law for compressible flows is:

$$\rho = \frac{p_{op} + p}{RT} \tag{24}$$

Where, p is the local gauge pressure predicted by FLUENT and p_{op} is the operating pressure.

For ideal gases, the dynamic viscosity μ is related to the absolute temperature T. Sutherland′s law was used to account for the change in viscosity with changing temperature. Sutherland's law was selected as it is suitable for simulating high speed compressible flows. It gives quite accurate results with minimum errors over a wide range of temperatures. Sutherland′s law can be expressed as:

$$\mu = \mu_{ref} \left(\frac{T}{T_{ref}}\right)^{\frac{3}{2}} \frac{T_{ref} + S}{T + S} \tag{25}$$

Where, $Tref$ is reference temperature and μref is the viscosity at the $Tref$ reference temperature.

2.9 Discrete Phase Boundary conditions

The copper particles of varying sizes were used in the simulation to see their effect on the outlet velocity. The varying sizes of copper particles were used with an initial velocity of 30 m/s and an initial temperature of 300 K. The powder mass flow rate

used for particle tracking was 10-15% less than the gas mass flow rate so that it would not disturb the gas flow field.

The following assumptions were made for DPM:

1) The copper particles were spherical in shape.

2) The particles introduced in the axial direction of the nozzle.

3) The particles were accelerated by the drag force of the gas used.

4) The temperature inside the copper particle was uniform.

For powder size distribution Rosin-Rammler diameter distribution method is used. If the size distribution is of the Rosin-Rammler type, the mass fraction of particles of diameter greater than d is given by:

$$Y_d = e^{-\left(\frac{d}{\bar{d}}\right)^n} \qquad (26)$$

Where 'n' is the size distribution parameter and d is the mean diameter of a particle.

Chapter 3

Results: 2D Spray Model

3.1 Geometry
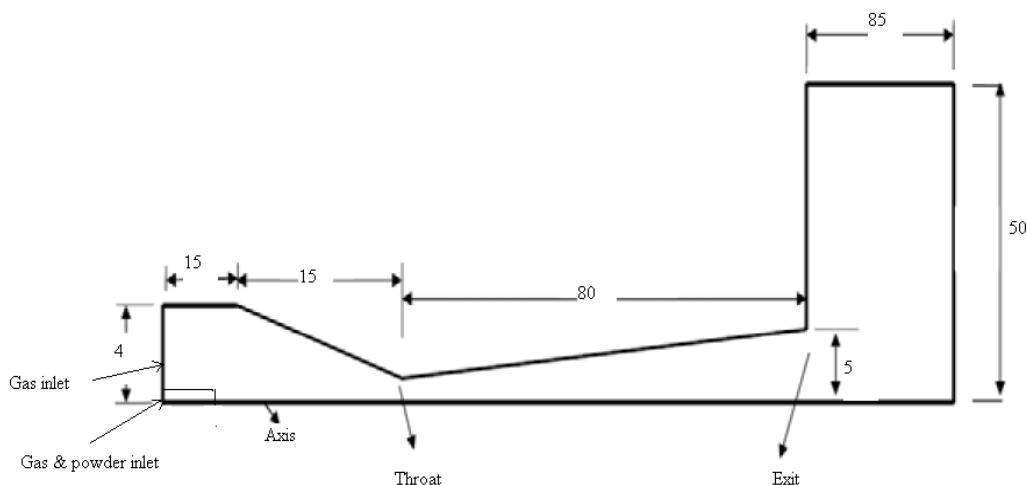
Figure 3.1: Geometry used for simulation

The 3.1 shows the dimensions of cold spray nozzle used for the simulation. The main aim of selecting this convergent-divergent nozzle is to attain the supersonic velocity of gas in the exit. A high pressure gas is preheated and led into a converging-diverging nozzle through the gas inlet. The cold spray copper powder is fed axially and centrally into the nozzle. In the divergent section, gas and powder particles are accelerated to supersonic velocity.

3.2 Meshing

Meshing is the first and foremost step for the simulation process. It includes finding the dimensions for the sprat gun and discretizing the domain into finite volume cells. Meshing has significant impact on rate of convergence, solution accuracy and CPU time.
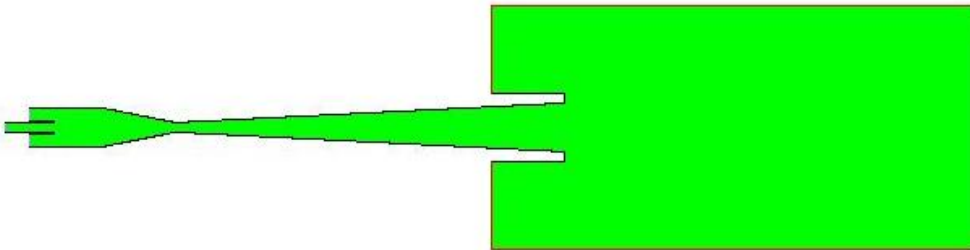
Figure 3.2: Computational Domain of Spray Gun created in ICEM-CFD

3.2.1 Meshing Procedure

Modelling has been done with the above dimensions and used the meshing tool of AnsysICEM CFD. After meshing the mesh was subjected to an quality testing and following results were obtained.

Mesh quality   : 0.9784 (it ranges from 0 to 1, close to zero as low quality)

Maximum aspect ratio : 3.858

Number of cells   : 54000 (after analyzing mesh independence)

3.3 Boundary conditions for Base case

Carrier Gas inlet	: Pressure inlet
Gas & powder inlet	: Pressure inlet
Gas outlet	: pressure outlet
Carrier Gas inlet pressure	: 21 bar
Outlet pressure	: atmospheric pressure
Carrier gas inlet temperature	: 473 K
Type of carrier gas used	: Helium
Injector & nozzle wall	: Adiabatic
Spray gun material	: Steel
Particle injection type	: Surface injection
Particle inlet temperature	: 300 K
Particle velocity at inlet	: 30m/s
Particle type	: Inert
Particle Material	: Copper
Diameter distribution	: Rosin-Rammler

Particle size distribution for base case

Diameter (microns)	10.9	14.5	18.7	22.7	25.9
Mass fraction	0.9	0.75	0.5	0.25	0.1

Mean size of particle   : 20.9 μm

3.4 Mesh Independence

To obtain an accurate solution, the platform at which the problem is simulated should be fine enough to get accurate values, meanwhile it should not take reasonable amount of computational effort. Initially four meshes were created and named mesh A, B, C and D in increasing order of their fineness.

Meshes created and changes in the particle velocity at the exit of the nozzle as shown below:

Mesh	Number of cells	Mean particle velocity (m/s)	% change in velocity
A	26000	635.72	-
B	54000	636.2	0.075
C	75000	636.59	0.136
D	100000	636.7	0.15

Grid independence

The above table.1 shows that the difference in velocity for using various grids was very small, so it was decided to use Mesh B for all 2D simulations as it is the best compromised between computational effort and accuracy.

3.5 Validation

It is important to validate the computational values before implementing them into the practical work and assessing their usefulness. Validation was performed by comparing the present CFD results with previously published experimental [43] results. Different applications require a different degree of accuracy in the

validation, so the validation process is flexible to allow for different degree of accuracy.

3.5.1 Validation With Experimental results
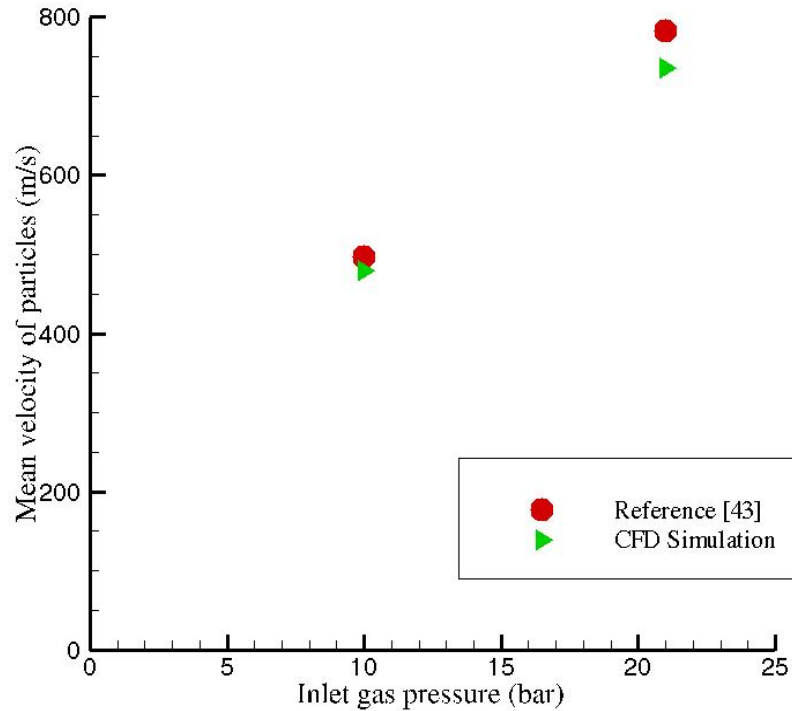
Figure 3.3: Validation with experimental results

The fig.3.2 shows the validation of simulation results with the experimental result [43]. For comparing with the experimental result, two inlet carrier gas pressures are considered for CFD simulation i.e. 10 bar and 21 bar. For the inlet gas pressure of 10 bar, the CFD simulation shows the mean particle velocity of 479.89 m/s, which is 3.44% less than experimental result [43]. For the inlet gas pressure of 21bar, the CFD simulation shows the mean particle velocity of 735 m/s, which is 6% less than the experimental result [43]. The variations are within the permissible limits, so the validation says to move further steps of simulation process.

45

3.6 Velocity Contours (Base case)

Fig.3.4 shows contour plot of velocity magnitude between the inlet and outlet regions. The injection port pressure was set to 31.69 bar, to generate a mass flow rate of approximately 20% of the main gas (carrier gas inlet) flow. This condition falls within the optimum range for the current Cold Spray system to generate a consistent powder flow from the feeder. The gas phase maximum velocity is 1800 m/s, which corresponds to a Mach number of 3.5. The nozzle is shown to be over-expanded and therefore oblique shock waves develop at the exit.

Fig.3.5 shows the changes in pressure along the length of the nozzle. The pressure of the gas is high till the throat of the nozzle, After that the gas starts expanding in the divergent part of the nozzle and therefore the pressure decreases. At the exit of the nozzle the gauge pressure becomes nearly zero, Due to over expansion of the gas phase at the nozzle exit, Shock waves are formed and therefore pressure fluctuations are seen. The changes in pressure and velocity due to shock waves are clearly shown in fig.3.6. Several oblique shock waves are seen after the exit of the convergent-divergent nozzle due to the expansion of the supersonic gas as seen in fig.3.6.
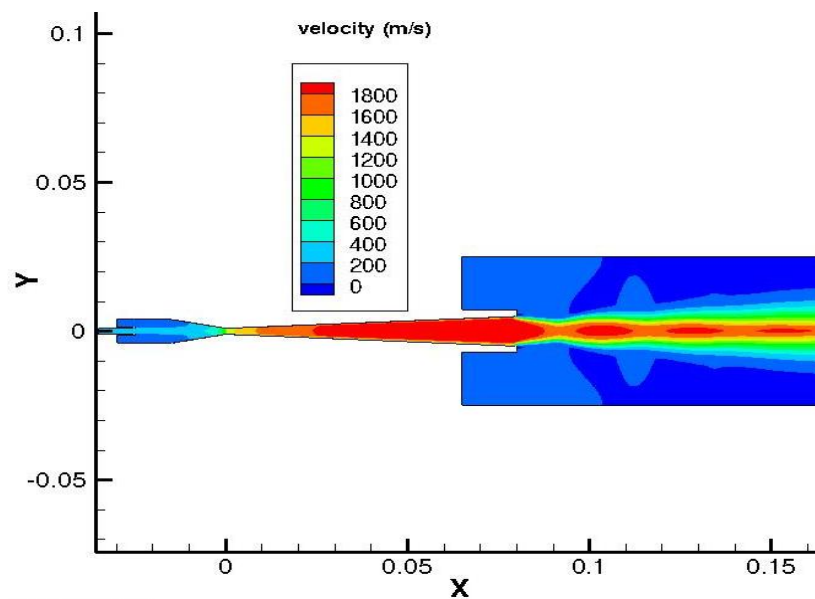
Figure 3.4: Velocity contour plot using helium as a carrier gas
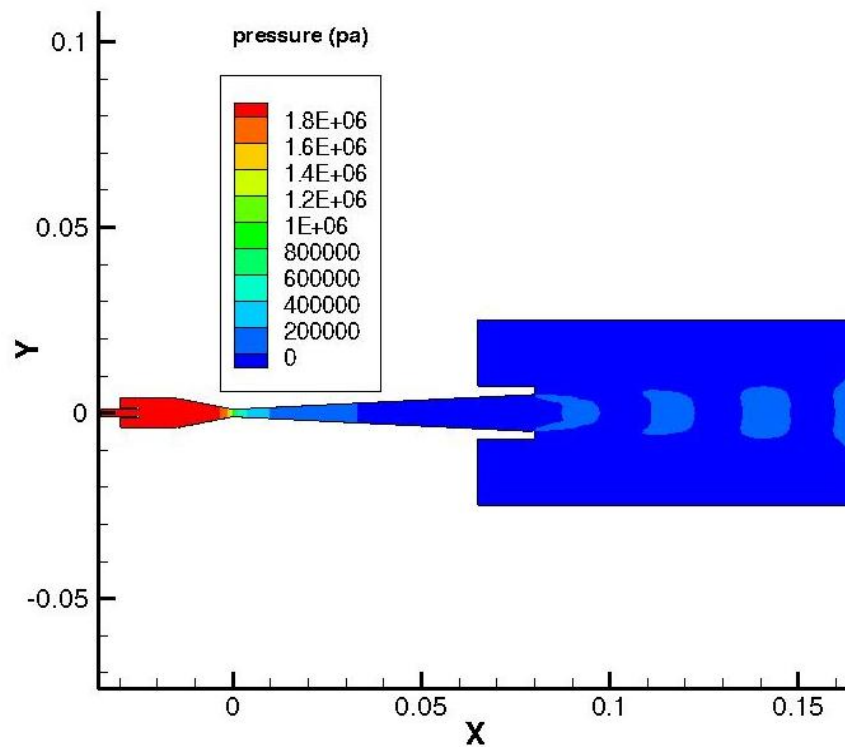
Figure 3.5: pressure contours
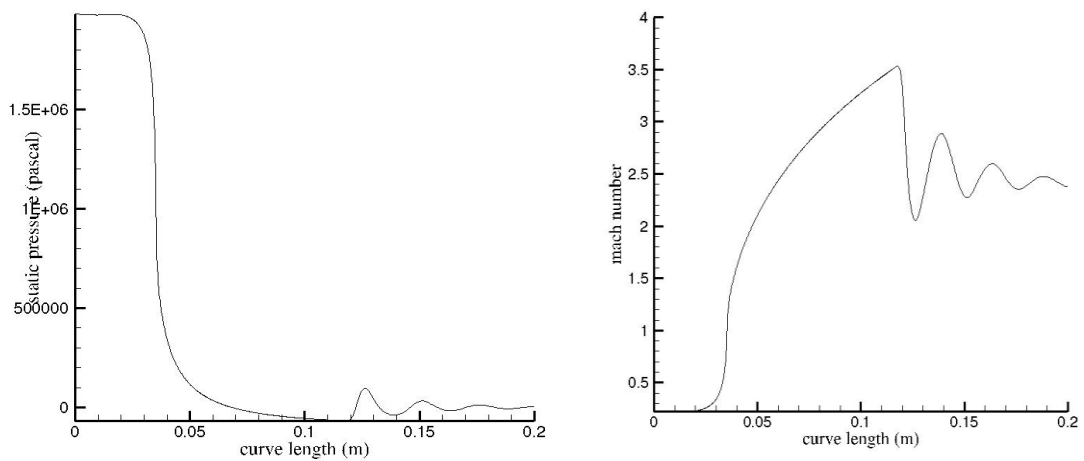
Figure 3.6: Profile of static pressure and Mach number distribution along the

nozzle axis

3.7 Parametric Study of Cold Spray Process

3.7.1 Effect of Various Carrier Gases on Particle velocity

In this case only changing the type of gas used for the simulation and keep all other conditions are same as in the base case. Three types of gases were used in the simulation to see their effect on the velocity on copper particles through the nozzle.

The three different gases used for the simulation are helium, nitrogen and argon. Out of three gases, helium is the lightest gas because its molecular weight is lowest compared to the other two gases. The molecular weight of helium, nitrogen and argon are 4, 28 and 39.948 respectively. Because of the lower molecular weight, helium gas attains almost three times the velocity of nitrogen and argon at the exit of the spray gun is shown in fig.3.7.
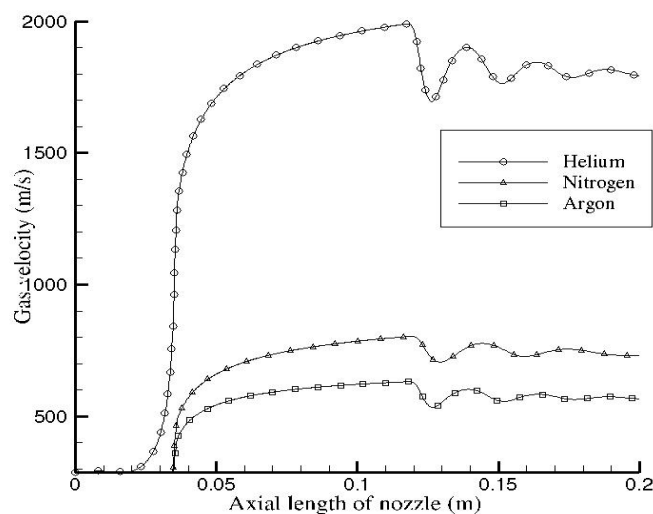
Figure 3.7: Velocity Variation of three Different Gases

Figs 3.8-3.10 shows the velocity profile along the axial length for different particle sizes when helium, nitrogen and argon are used as carrier gas. When helium is used it imparts the highest particle velocity compared to nitrogen and argon. It can be
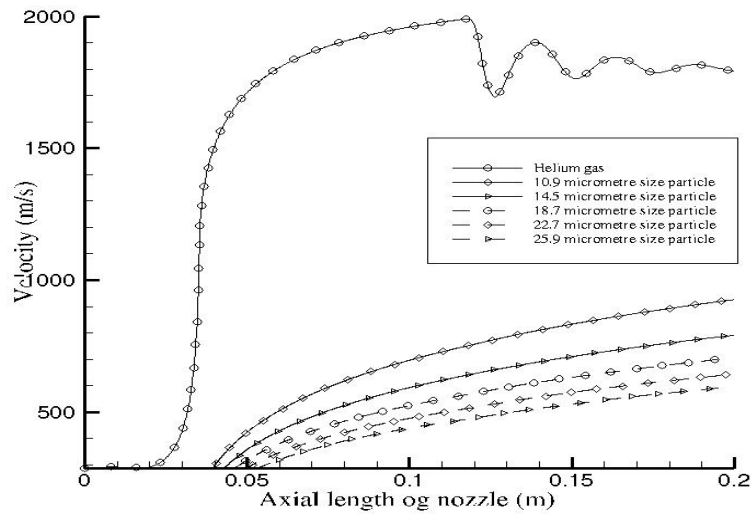
Figure 3.8: Velocity Variation of Particles by Using Helium as a Carrier Gas

seen that there is an increase in particle velocity upto 200 m/s in the case of helium as compared to nitrogen.
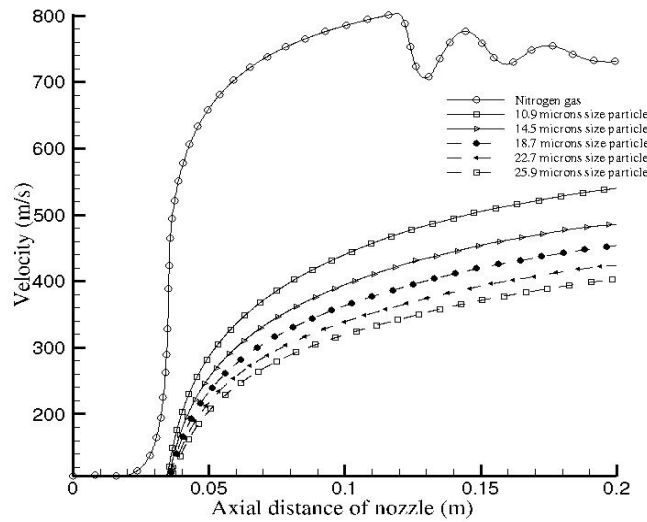

Figure 3.9: Velocity Variation of Particles by Using Nitrogen as a Carrier Gas

The Figs 3.8-3.10 shows that the particles reach approximately 42% of the gas velocity when helium is used, 60% of gas velocity when nitrogen is used and 70% when argon is used. Since the drag imparted to the particle improves with increasing molecular weight of the carrier gas, however, particles in helium has the highest

49

velocity as the carrier gas has the highest velocity. Because of higher particle velocity by using by using helium results in a deposition efficiency of 75% as compared to 30 to 35% when using nitrogen or argon as a carrier gas.
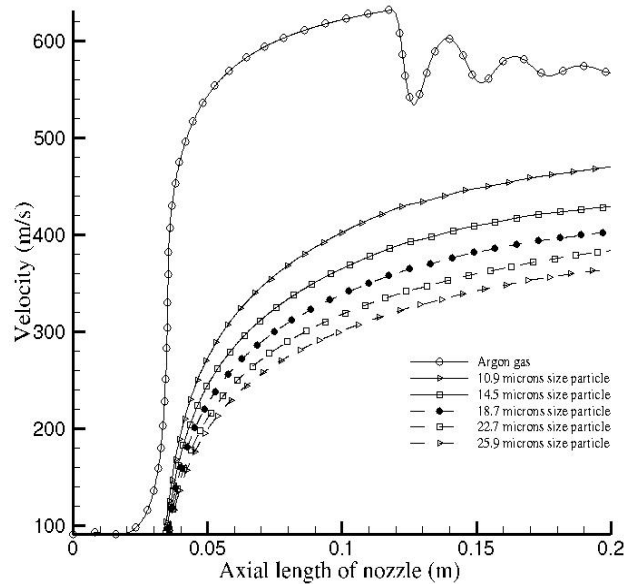
Figure 3.10: Velocity Variation of Particles by Using Argon as a carrier Gas

Fig.3.11 shows the mean particle velocity by using various carrier gases. In that curve clearly shows the particles achieve very high velocity by using helium as a carrier gas as compared to nitrogen and argon.
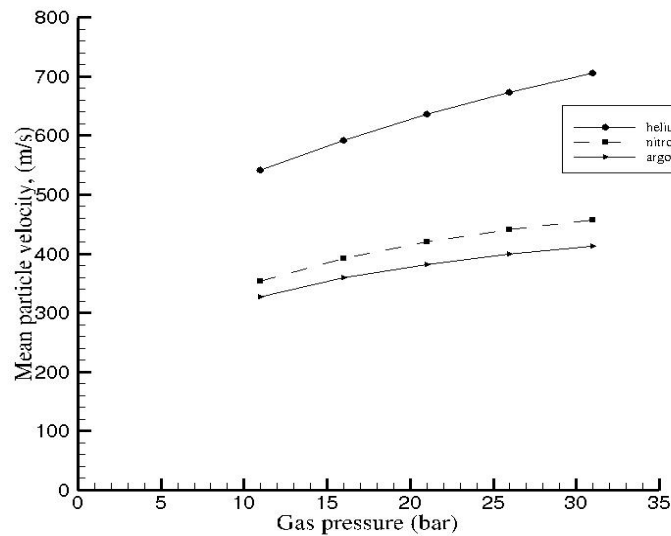

Figure 3.11: Effect of Carrier Gases on Mean Particle Velocity

The figs 3.8-3.10 Show that the particles of different sizes have different velocities. Velocities of the particles decrease with increase in particle size because acceleration due to drag on the particles depends on mass of the particles. So the lighter particles travel with higher velocity as compared to heavier particles.

3.7.2 Effect of Gas Temperature on Particle Velocity

In this case only changing the temperature of gas used for the simulation and keep all other conditions are same as in the base case.
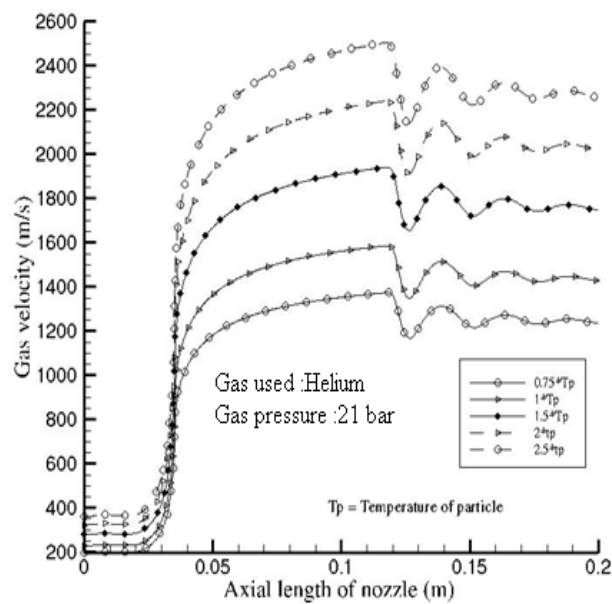
Figure 3.12: Effect of Gas Temperature on Gas Velocity

The deposition efficiency of particles depends upon the temperature of the carrier gas. It was reported earlier [25] that when nitrogen is used to spray titanium particles the critical temperature is 155 °C, below this temperature no particle deposition took place. When the temperature was further increased, the deposition efficiency also increased rapidly, especially when the temperature of nitrogen exceeded 215 °C. The reason behind the above statement is the critical velocity is a function of the temperature of carrier gas .

Fig.3.12 shows the increase in carrier gas velocity by changing the carrier gas temperature. As the temperature of carrier gas is increased the velocity of particles

also increase and it should result in higher deposition efficiency of the particles on the substrate.

Fig3.13 shows the variation in particle velocity at the outlet with varying gas temperature. As discussed earlier, switching from a carrier gas with higher molecular weight to one with lower molecular weight like helium results in increase in the mean particle velocity. In the same manner increase in gas inlet temperature results in decrease in gas density, therefore the overall drag on the particles increases.
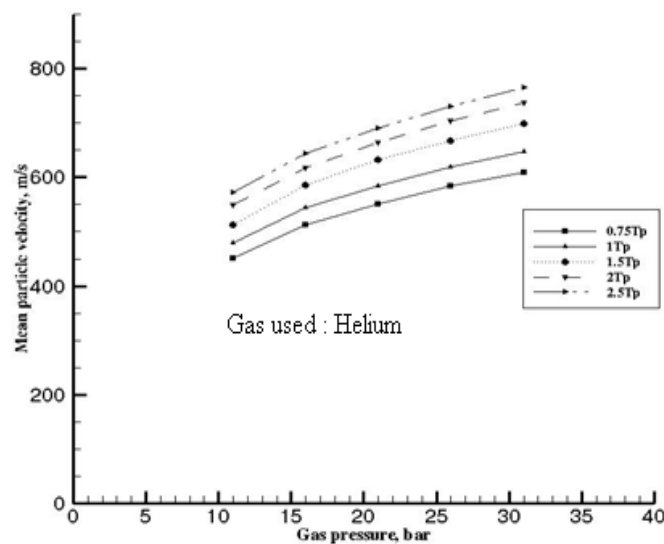
Figure 3.13: Effect of Carrier Gas Temperature on Mean Particle Velocity

3.7.3 Effect of Gas Pressure on Mean Particle Velocity

In this case only changing the inlet pressure of carrier gas used for the simulation and keep all other conditions are same as in the base case

The fig 3.14 shows the effect of changing the inlet pressure of carrier gas used for simulation. The variation in outlet gas velocity by changing the inlet carrier gas pressure is less as compared to changing carrier gas inlet temperature. But the

particle velocity in the outlet increases, because increasing the inlet carrier gas increase the density of gas, so the drag on the particle increases.
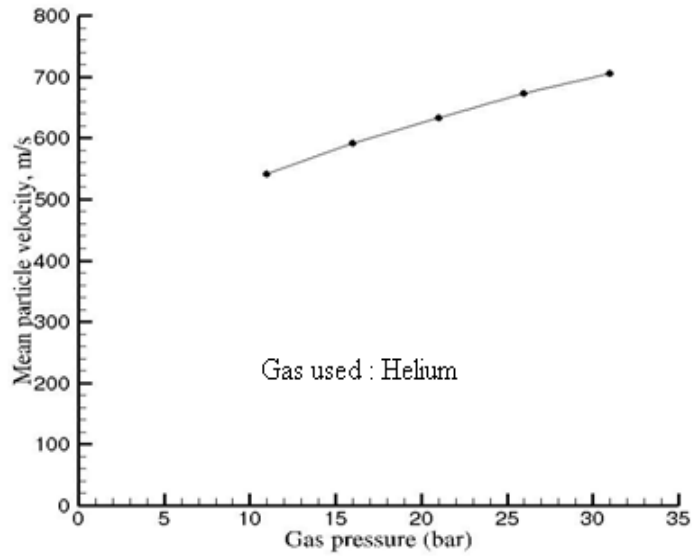

Figure 3.14: Effect Gas Pressure on Mean Particle Velocity

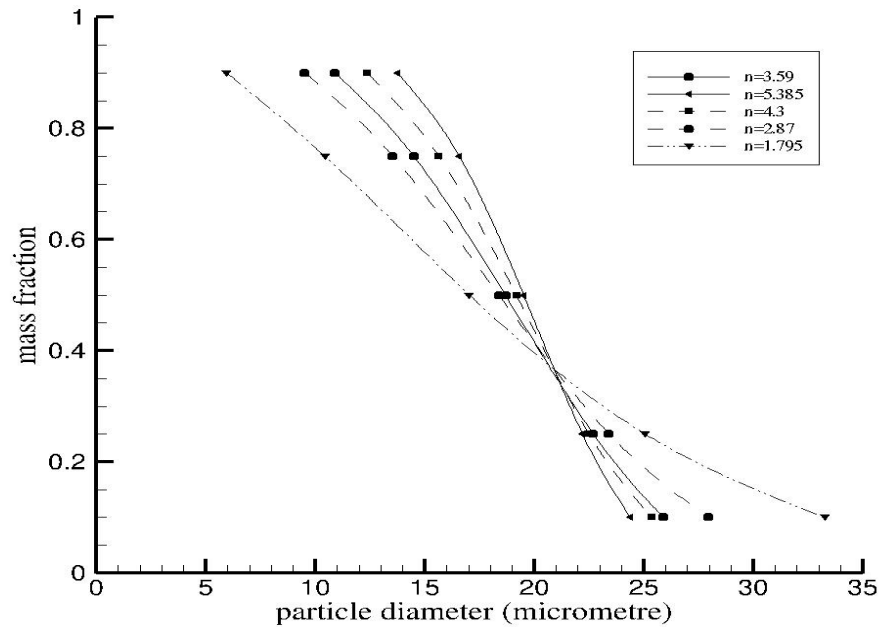## 3.7.4 Effect of Particle Size on Mean Particle Velocity

Figure 3.15: Various Particle Size Distribution

The Rosin-Rammler distribution function is used for calculating the size distribution of particles. In Rosin-Rammler distribution the parameter 'n' called the spread parameter, by changing this parameter 'n' and finding various size distributions. If the parameter 'n' is increased, it will increase the difference between the diameter range of particles, and if the parameter 'n' is decreased the difference is increased is shown in fig.3.15
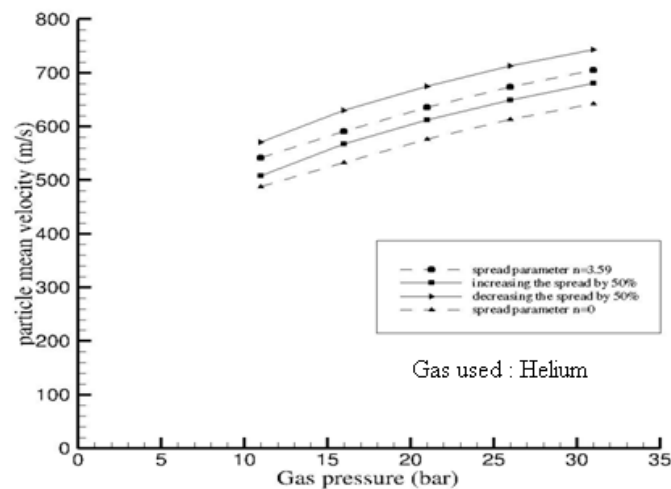

Figure 3.16: Effect Particle Size Distribution on Mean Particle Velocity

Fig.3.16 shows the particle velocity in outlet by using various size distribution of particles. If the size distribution parameter 'n' is decreased, then the particle distribution have smaller particles as well as larger particles but the smaller particles have larger in number, this is the reason for increasing the mean velocity of particles in the outlet. If the parameter 'n' is increased, the particle velocity in the outlet was decreased.

3.8 DPM Concentration in the Outlet at Various Locations

Fig.3.17 shows the DPM Concentration (concentration of particles) at various radial locations at the outlet of the nozzle. It shows that DPM concentration is least when helium is used as carrier gas, because helium gas attain almost 3 times the velocity

of nitrogen and argon at the outlet, so large amount of dispersion of particles takes place in the outlet of the spray gun.
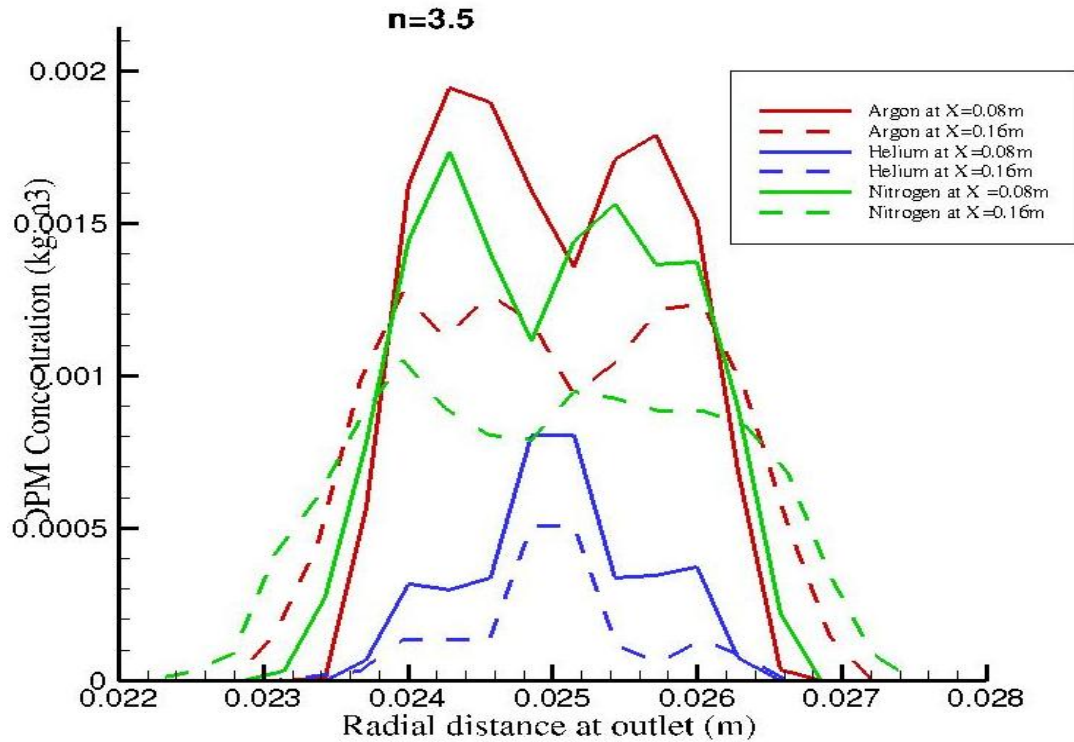

Figure 3.17: DPM Concentration at Radial Distance in the Outlet

If there is large dispersion, then the width should increase. The real reason might be because, as the mass flow rate of particle is a prescribed value and the particle attains very high values, the overall concentration and the width of the cross-section occupied by the particles should decrease due to mass conservation. The fig.3.17 also shows the DPM concentration is higher when argon is used as carrier gas in comparison with nitrogen because the argon velocity is low in the outlet compared to nitrogen, so the dispersion of particles is less compared to nitrogen

3.8 Turbulence

Fig 3.18 shows the production of turbulent kinetic energy due to turbulence throughout the flow field. The turbulent kinetic energy is produced due to velocity gradients in the flow. The fig 3.18 shows at 0.2 sec the production of turbulent kinetic energy is high and after that (at t=0.6 sec) it will be reduced because the

perturbations in the flow will be reduced and the flow becomes stable after some time.
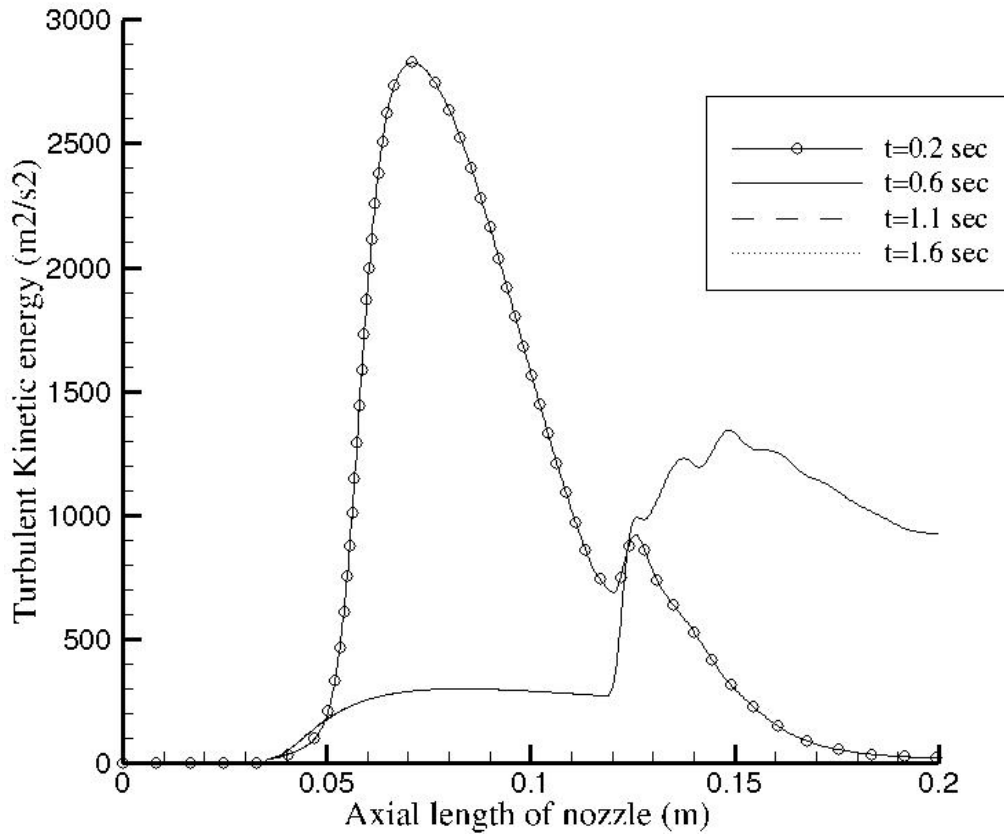

Figure 3.18: Production of Kinetic Energy due to Turbulence

Fig 3.19 Shows the dissipation of kinetic energy due to turbulence. In turbulent flow the dissipation of energy means that kinetic energy in the small (dissipative) eddies are transformed into internal energy. The small eddies receive kinetic energy from slightly larger eddies. The slightly larger eddies receive their energy from even larger eddies and so on. The largest eddies extract their energy from the mean flow. This process of transferred energy from the largest turbulent scales (eddies) to the smallest is called cascade process. The fig 3.19 shows at the beginning (at t=0.2 sec) the dissipation is high and after that constant.
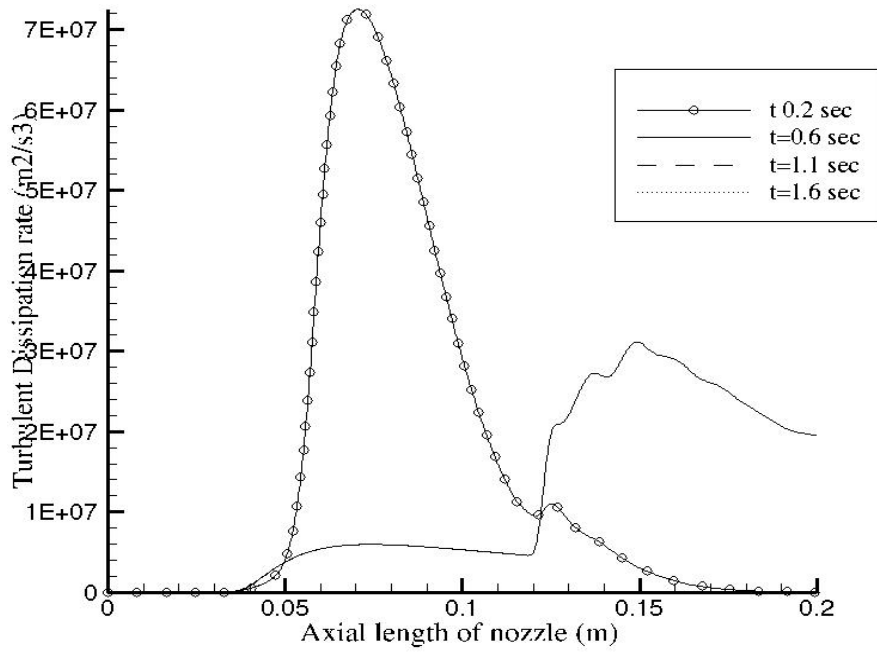
Figure 3.19 : Dissipation of Turbulent Kinetic Energy

Fig 3.21 shows the production of turbulent kinetic energy in radial distance at the outlet due to turbulence. It shows the production of kinetic energy is less in the centre of jet and high at the surface of the jet.
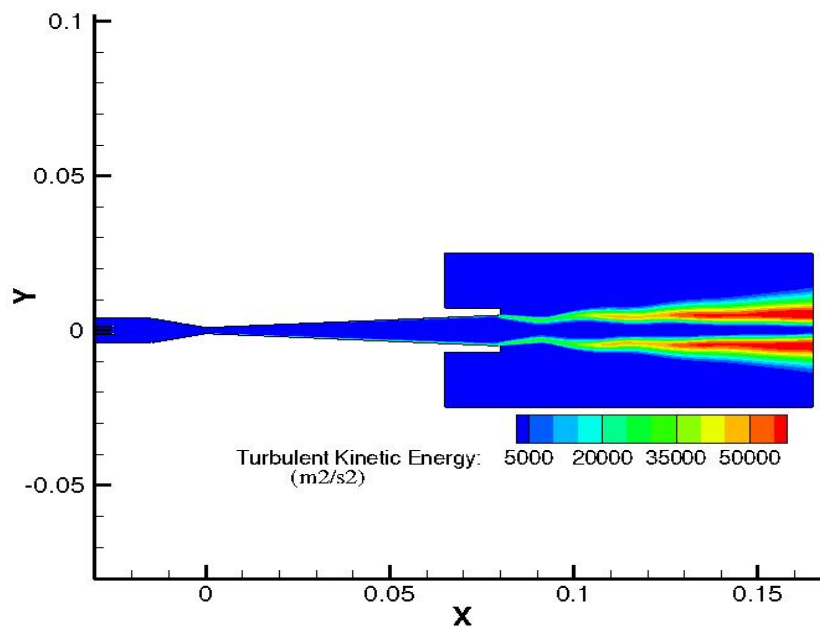

Figure 3.20 : Contours of Turbulent Kinetic Energy production.

The turbulent kinetic energy is produced due to shear stress in the flow field. The shear stress is produced due to velocity gradient in the jet. The velocity gradient is very less at the centre of the jet and high at the surface, so the shear stress is high at the surface and less at the centre of the jet. This is the reason the turbulent kinetic energy is high at the surface of the jet and very less (nearly zero) at the centre of the jet.
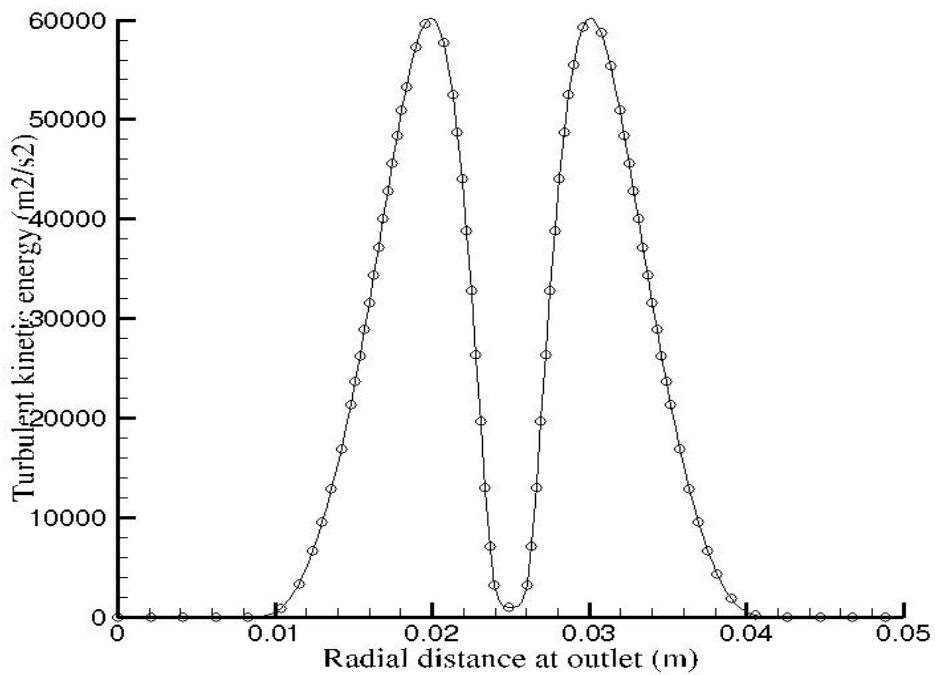

Figure 3.21: Production of Turbulent Kinetic Energy due to turbulence in radial distance at the outlet.

Chapter 4

Results: 3D Spray Model

4.1 Computational Domain

For 3D spray model three different sizes of mesh were created and named as A, B and C respectively. The mesh A contains 386000 cells, mesh B as 780000 cells and mesh C as 1426000 cells. At the time of running the simulation the mesh A get diverged and mesh B gives the wrong result, this is because simulating with DES turbulence model very fine grid is required. So choose mesh C as the final mesh for running all the simulations is shown in fig 4.1.
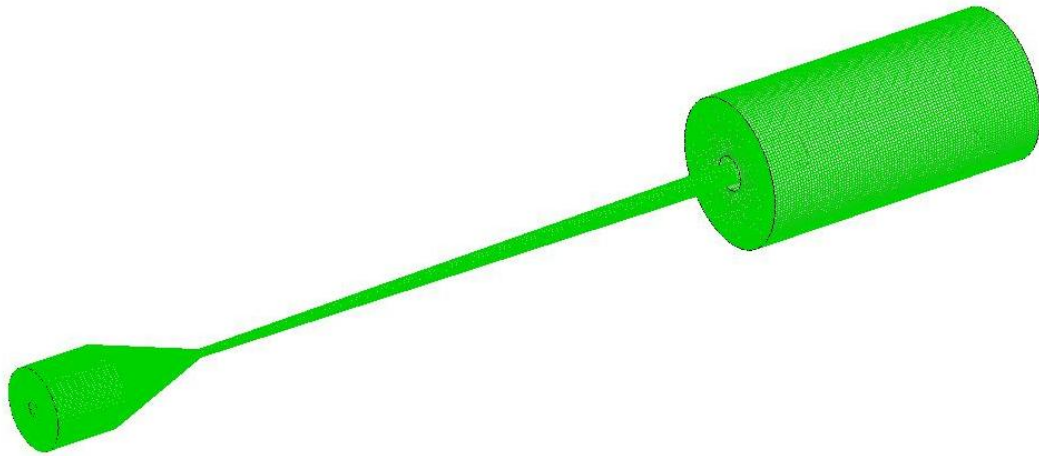

Figure 4.1: Computational Domain for 3D Spray Model

4.2 Velocity contour

The fig.4.2 shows the velocity contour of the 3d spray model. In that contour the velocity is fluctuating in the outlet, this is because of overexpansion of gases. The

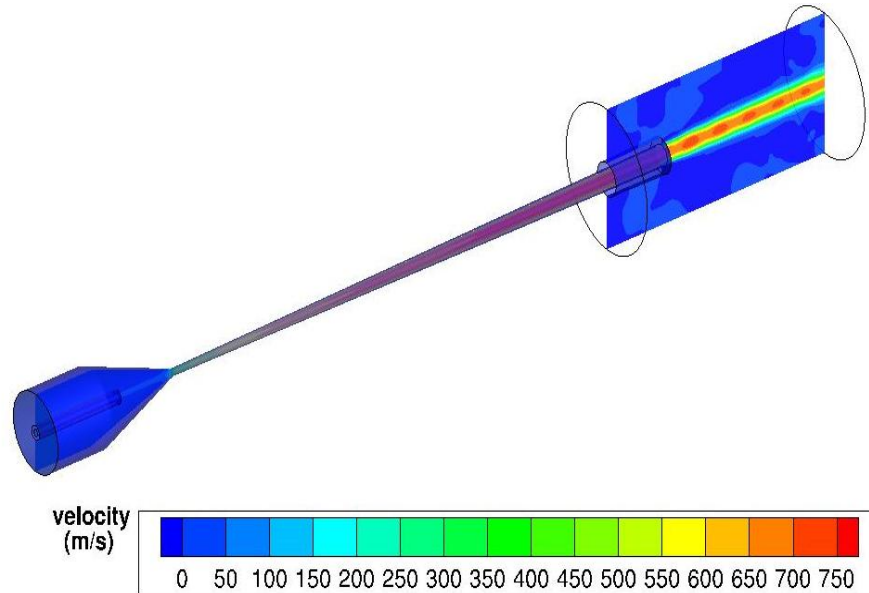over expansion of gases in the outlet creates the shock waves, so the velocity is fluctuating in the outlet.

Figure 4.2: Velocity contour of 3d spray model.

4.3 Uncoupled and Coupled Calculations

For the uncoupled calculation, we will perform the following two steps:

1) Solve the continuous phase flow field.
2) Plot the particle trajectories for discrete phase injections of interest.

This procedure is adequate when the discrete phase is present at a low mass and momentum loading, in which case the continuous phase is not impacted by the presence of the discrete phase.

In a coupled two-phase simulation, ANSYS FLUENT modifies the two-step procedure above as follows:

1) Solve the continuous phase flow field (prior to introduction of discrete phase).

60

2) Introduce the discrete phase by calculating the particle trajectories for each discrete phase injection.

3) Recalculate the continuous phase flow, using the interphase exchange of momentum, heat and mass determined during the previous particle calculation.

4) Recalculate the discrete phase trajectories in the modified continuous phase flow field.

5) Repeat the previous two steps until a converged solution is achieved in which both the continuous phase flow field and the discrete phase particle trajectories are unchanged with each additional calculation.

The fig.4.3 shows the jet velocity variation due to coupled and uncoupled approach
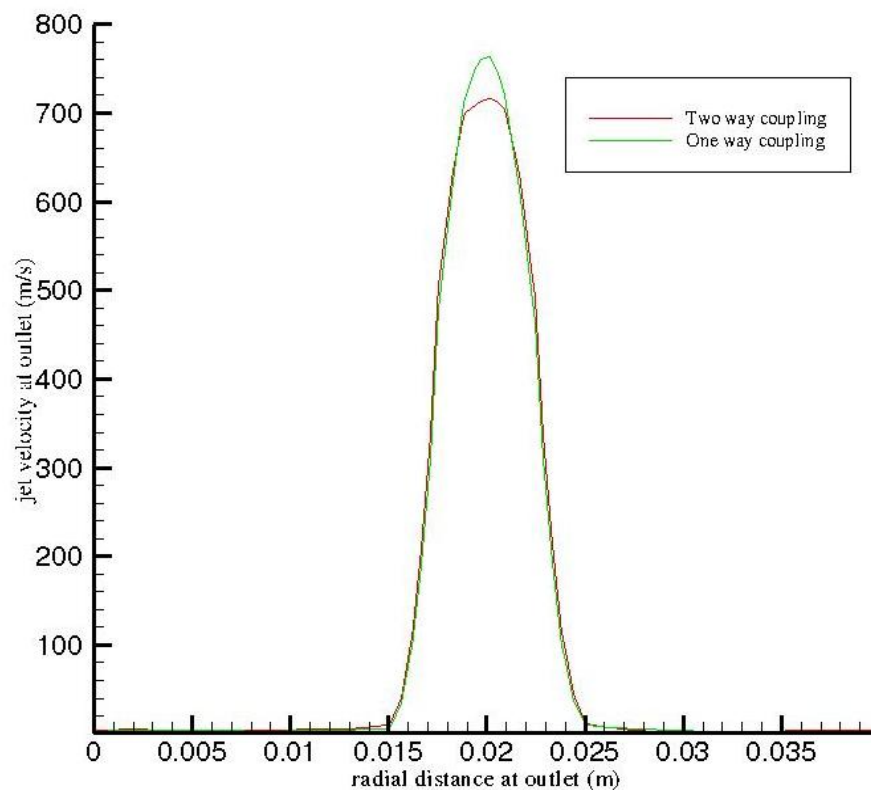

Figure 4.3: Jet Velocity Variation at Outlet due to Coupled and Uncoupled Approach.

4.4 Gas velocity & Particle Concentration in the Outlet at Various Radial Distance

Fig.4.4 shows the carrier gas velocity at various radial locations in the outlet of a spray gun. It shows the carrier gas velocity high in the centre of the spray gun.
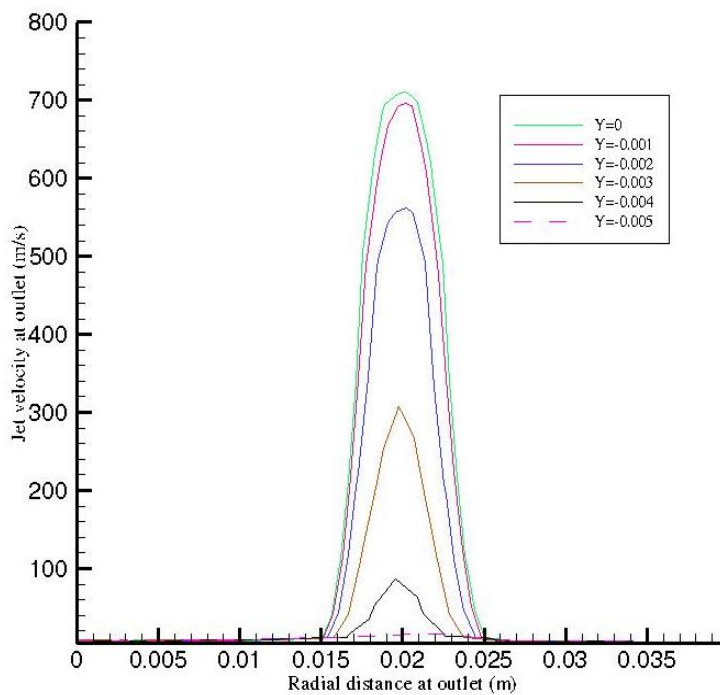

Figure 4.4: Gas Velocity in the Outlet at Various Radial Locations

The fig.4.5 shows the concentration of particles at various radial locations in the outlet of the spray gun. The curve clearly shows majority of particles are accumulated in the centre line of the spray gun. The fig 4.4 shows the gas velocity also very high in the centre, therefore the drag on the particle is high in the centre line. So the particle accumulated in the centerline of the spray gun will achieved a very high velocity compared to the particles away from the centerline
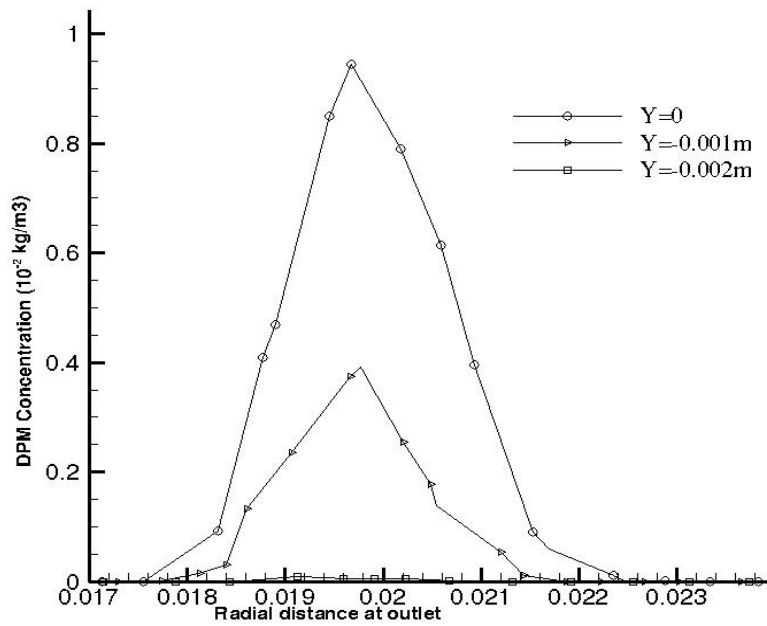
Figure 4.5: DPM Concentration at various radial location at outlet

.

4.5 Turbulent Kinetic Energy

Fig.4.6 shows the production of turbulent kinetic energy in the radial distance at x=0.2m from the nozzle inlet.
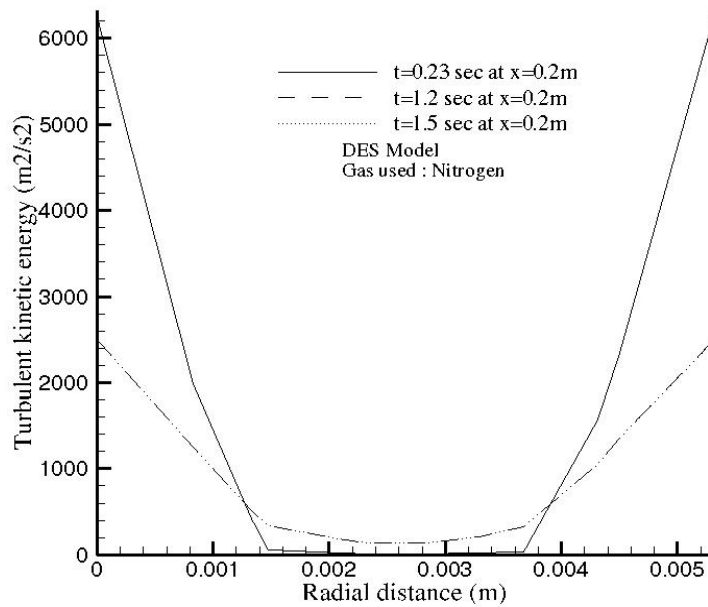

Figure 4.6: Production of Turbulent Kinetic energy in the radial distance at x=0.2m and varying the time.

The turbulent kinetic energy is produced due to shear stress in the flow field. In the wall region the total shear stress is approximately constant and equal to wall shear stress(τ_w). The total stress constant only close to the wall; further away from the wall it decreases linearly. At the wall the turbulent stress vanishes as u=v=0 and away from the wall it will be increases. The production of kinetic energy is varied based on the shear stress only.

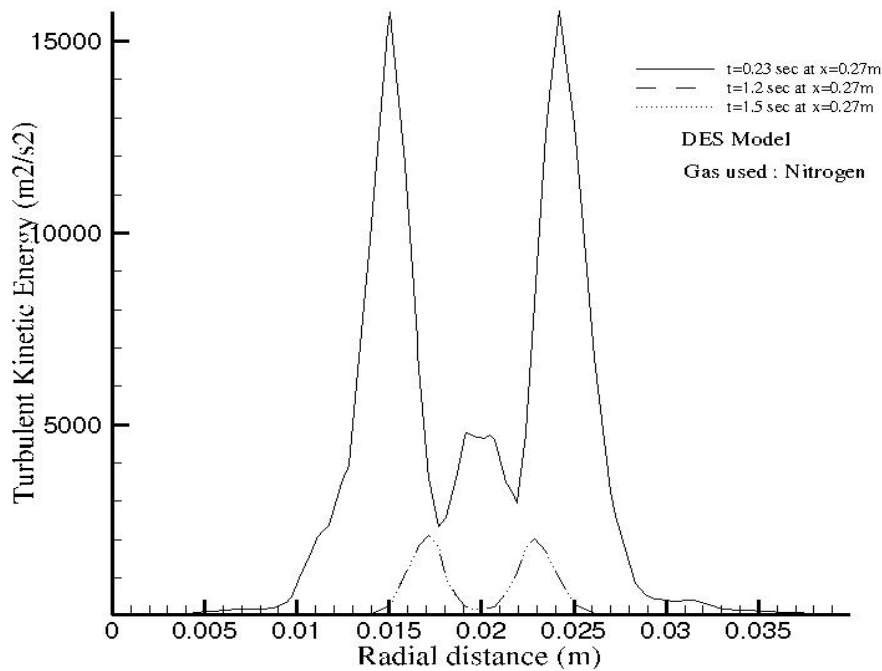
Figure 4.7: Production of Turbulent Kinetic energy in the radial distance at x=0.27m and varying the time.

Fig. 4.7 shows the production of turbulent kinetic energy at various radial location in the outlet. It shows the kinetic energy is high near the surface of the jet, the reason is the velocity gradient is high near the surface . so the shear stress is high near the surface of the jet.

Conclusions

The velocity of copper particles achieved in a cold spray nozzle were analysed with different particle size distributions, different gases, different gas pressure & temperature, one way & two way couplings and different turbulence models using CFD simulations. The simulation results showed that:

- The Mach number of the gas increases with a decrease in pressure along the axis of the nozzle. This results in greater gas velocity toward the nozzle exit.

- The results show that by increasing the gas temperature increases the gas velocity more significantly than the gas pressure, which shows that the gas velocity is a function of gas temperature and not the gas pressure.

- The results shows the particle size distribution plays a major role in the particle exit velocity i.e. lighter particles travels much faster than heavier particles.

- In the simulation argon, nitrogen and helium were used for spraying copper particles. Results show that helium is a far better carrier gas because particles achieve much higher velocity when helium is used for spraying.

- The temperature of the gas influences the velocity of copper particles because the density of gas decreases with increasing gas temperature and hence there is a greater gas velocity to accelerate the copper particles.

- Increasing the applied gas pressure increase the density of the gas which results in more drag on the particles. Increasing gas pressure does not affect the velocity of gas.

- The 2d analysis does not shows any difference between one way & two way coupling but the 3d analysis shows some difference in particle velocity.

- The turbulence analysis shows the turbulent activity is high at the starting time of the flow after that it will be reduced and the flow becomes stable.

- The turbulence analysis also shows the production of turbulent kinetic energy is high in area where large velocity gradient .

References

[1]   Tobias Schmidt, Hamid Assadi, Frank Gartner, Horst Richter, Thorsten Stoltenhoff, Heinrich Kreye, and Thomas Klassen, From Particle Acceleration to Impact and Bonding in Cold Spraying, Journal of Thermal Spray Technology, JTTEE 18, 2009, p. 794-808

[2]   Tiziana Marrocco, Cold Spray Technology from TWI, TWI Technology Centre (Yorkshire), 2007

[3]   V.F. Kosarev, S.V. Klinkov, A.P. Alkhimov, and A.N. Papyrin, On some aspects of gas dynamic of the cold spray process, ASM international, 2003, JTTEE5 12:265-281

[4]   J. Karthikeyan, Cold spray technology: International status and USA efforts, ASB Industries, Inc., december 2004

[5]   P. Fauchais, A. Vardelle, and B. Dussoubs, Quo Vadis Thermal Spraying, ASM International, JTTEE 10, 2001, p. 44-66

[6]   C.-J. Li and A. Ohmori, Relationships Between the Microstructure and Properties of Thermally Sprayed Deposits, Journal of Thermal Spray Technology, JTTEE5 11, 2002, p. 365-374

[7]   Cast steel: Advances in Thermal Spray Technology, http://www.keytometals.com/Articles/Art138.htm, 2010, p. 1-2

[8]   Jin Kawakita a,□, Hiroshi Katanoda b, Makoto Watanabe a, Kensuke Yokoyama a, Seiji Kuroda a, Warm Spraying: An improved spray process to deposit novel coatings, Surface & Coating Technology, 202, 2008, p. 4369-4373

[9]   Thermal spray products, file:///F:/27April/thermalsprayprocesses.html, Metallisation

[10]   J. Karthikeyan, Evolution of cold spray technology, http://www.entrepreneur.com/tradejournals/article/print/146546589.html, 2010

[11]   G. D. Davis*, G. B. Groff, R. A. Zatorski, Plasma Spray Coatings as Treatments for Aluminum, Titanium and Steel Adherends, Surface and Interface Analysis, VOL. 25, 1997, p. 366-373

[12]   Rainer Gadow, Andreas Killinger, and Johannes Rauch, Introduction to High-Velocity Suspension Flame Spraying (HVSFS), Journal of Thermal Spray Technology, JTTEE5 17, 2008, p. 655-661

[13] Mingheng Li, Panagiotis D.Christofides, Multi-scale modelling and analysis of an industrial HVOF thermal spray process, Journal of chemical Engineering Science, 60, 2005, p.3649-3669.

[14] J. Rauch, G. Bolelli, A. Killinger, R. Gadow, V. Cannillo, L. Lusvarghi, Advances in High Velocity Suspension Flame Spraying (HVSFS), Journal of thermal spray technology, JTTEE 15, 203, 2009, 2131-2138

[15] Sergei Vladimirovich Klinkov, Vladimir Fedorovich Kosarev, Martin Rein, Cold spray deposition: Significance of particle impact phenomena,Journal of Thermal spray technology, JTTEE, 9, 2005, p. 582-591

[16] Anatolii Papyrin, Vladimir Kosarev, Sergey Klinkov, Anatolii Alkhimov, Vasily Fomin, Cold Spray Technology, JTTEE 12, 2007

[17] F. Gärtner, T. Schmidt, T. Stoltenhoff and H. Kreye, Recent Developments and Potential Applications of Cold Spraying, Wiley Inter Science, 8 no.7, 2006, 611-618

[18] Frank Gaertner, Tobias Schmidt, Heinrich Kreye, Present Status and Future Prospects of Cold Spraying, Trans Tech Publications, Switzerland, vols. 534-536, 2007, p. 433-436

[19] R.E. Blose, B.H. Walker, R.M. Walker, S.H. Jroes, New opportunities to use cold spray process for applying additive features to titanium alloys, ASME, 2006, p. 30-37

[20] Vladimir F. Kosarev*, Sergey V. Klinkov and Aleksey A. Sova, Recently Patented Facilities and Applications in Cold Spray Engineering, Bentham Science Publishers Ltd, 2007, p. 35-42

[21] T. Stoltenhoff, H. Kreye, and H.J. Richter, An Analysis of the Cold Spray Process and Its Coatings, Journal of Thermal Spray Technology, JTTEE5 11, 2002, p. 542-550

[22] T. Han, B.A. Gillispie, and Z.B. Zhao, An Investigation on Powder Injection in the High-Pressure Cold Spray Process, Journal of Thermal Spray Technology, JTTEE5 18, 2009, p. 320-330

[23] Saden H. Zahiri, William Yang, and Mahnaz Jahedi, Characterization of cold spray titanium supersonic jet, Journal of Thermal Spray Technology, JTTEE5 18, 2009, 110-117

[24] Wen-Ya Li and Chang-Jiu Li, Optimal design of a novel cold spray gun nozzle at a limited space, Journal of Thermal Spray Technology, JTTEE5 14, 2005, 391-396

[25] T. Schmidt, F. Gaertner, and H. Kreye, New Development in Cold Spray Based on Higher Gas and Particle Temperature, Journal of Thermal Spray Technology, JTTEE5 15, 2006, 488-494

[26] M Grujicic, W S DeRosset and D Helfritch, Flow analysis and nozzleshape optimization for the cold-gas dynamic-spray process, ProQuest Science Journals, 217 part B, 2003, p. 1603-1613

[27] M. Fukumoto, M. Mashiko, M. Yamada, and E. Yamaguchi, Deposition Behavior of Copper Fine Particles onto Flat Substrate Surface in Cold Spraying, Journal of Thermal Spray Technology, JTTEE5 19, 2010, 89-94

[28] T. Van Steenkiste and J.R. Smith, Evaluation of Coatings Produced via Kinetic and Cold Spray Processes, Journal of Thermal Spray Technology, JTTEE5 13, 2004, p. 274-282

[29] Victor K. Champagne, The Repair of Magnesium Rotorcraft Components by Cold Spray, ASME, 2008, p. 164-175

[30] V. Shukla, G.S. Elliott, and B.H. Kear, Nanopowder Deposition by Supersonic Rectangular Jet Impingement, Journal of Thermal Spray Technology, JTTEE 59, 2000, p. 394-398

[31] J.G. Legoux, E. Irissou, and C. Moreau, Effect of Substrate Temperature on the Formation Mechanism of Cold-Sprayed Aluminum, Zinc and Tin Coatings, Journal of Thermal Spray Technology, JTTEE5 16, 2007, p. 619-627

[32] X. Luo · G. Wang · H. Olivier, Parametric investigation of particle acceleration in high enthalpy conical nozzle flows for coating applications, ASME, 2008, 351-362

[33] John D. Anderson, Modern Compressible Flow, Third Edition, McGraw- Hill Companies, Inc., p. 228-229

[34] C. S. JOG, Fluid Dynamics, Second Edition, volume-2, Alpha Science International Ltd., p. 412-414

[35] B. Jodoin, Cold Spray Nozzle Mach Number Limitation, Journal of Thermal Spray Technology, JTTEE5 11, 2002, p. 496-507

[36] Cold spray, file://E:\mass flow rate\mm_mp_ct_cs.html, Applied Research Laboratory at Penn State, 2010, p. 1-4

[37] M. Grujicic, J.R. Saylor, D.E. Beasley, W.S. DeRosset, D. Helfritch, Computational analysis of the interfacial bonding between feed-powder particles and the substrate in the cold-gas dynamic-spray process, JTTEE 41, 219, 200, p. 211-227

[38] R. Morgan*, P. Fox, J. Pattison, C. Sutcliffe, W. O"Neill, Analysis of cold gas dynamically sprayed aluminium deposits, ASME, 58, 2004, p. 1317- 1320

[39] Wen-Ya Li *, Hanlin Liao, G. Douchy, C. Coddet, Optimal design of a cold spray nozzle by numerical analysis of particle velocity and experimental validation with 316L stainless steel powder, Journal of thermal spray technology, JTTEE 7, 2007, p. 2129-2137

[40] Introduction to Fluent Inc., Chapter 2, 2006, 2-(1-2)

[41] B. Samareh, A. Dolatabadi, A Three-Dimensional Analysis of the Cold Spray Process: Effect of Substrate Location and Shape, Concordia University, Montreal

[42] Y. Li, A. Kirkpatrick, C. Mitchell, B. Willson, Characteristics and Computational Fluid Dynamics Modelling of High-Pressure Gas Jet Injection, ASME, vol. 126, January 2004, p. 192-198

[43] R.Lupoi, W.O'Neill, Powder stream characteristics in cold spray nozzles, Surface and Coatings Technology, 206(2011), p. 1069-1076.

[44] D.L.Gilmore, R.C.Dykhuizen, R.A.Neiser, T.J.Roemer,and M.F.Smith, Particle velocity and deposition efficiency in the cold spray process, JTTEE5:576-582